JOURNAL OF GEOPHYSICAL RESEARCH, VOL. 97, NO. C7, PAGES 11,453–11,469, JULY 15, 1992

Bound Infragravity Waves

MICHELE OKIHIRO, R. T. GUZA, AND R. J. SEYMOUR

Scripps Institution of Oceanography, University of California, San Diego, La Jolla

Model predictions of bound (i.e., nonlinearly forced by and coupled to wave groups) infragravity wave energy are compared with about 2 years of observations in 8- to 13-m depths at Imperial Beach, California, and Barbers Point, Hawaii. Frequency-directional spectra of free waves at sea and swell frequencies, estimated with a small array of four pressure sensors, are used to predict the bound wave spectra below 0.04 Hz. The predicted total bound wave energy is always less than the observed infragravity energy, and the underprediction increases with increasing water depth and especially with decreasing swell energy. At most half, and usually much less, of the observed infragravity energy is bound. Bound wave spectra are also predicted with data from a single wave gage in 183-m depth at Point Conception, California, and the assumption of unidirectional sea and swell. Even with energetic swell, less than 10% of the total observed infragravity energy in 183-m depth is bound. Free waves, either leaky or edge waves, are more energetic than bound waves at both the shallow and deep sites. The low level of infragravity energy observed in 183-m depth compared with 8- to 13-m depths, with similarly moderate sea and swell energy, suggests that leaky (and very high-mode edge) waves contribute less than 10% of the infragravity energy in 8–13 m. Most of the free infragravity energy in shallow water is refractively trapped and does not reach deep water.

1. INTRODUCTION

Infragravity waves are believed to be an important factor in several nearshore processes. The purpose of this paper is to estimate the contribution of bound waves to infragravity energy observed well outside the surf zone in depths of both ~10 and ~200 m. Infragravity motions (typical periods of 25–200 s on Pacific coasts) coupled to incident wave (typical periods of 4–25 s) groups were first observed in roughly 15 m depth by *Munk* [1949] and *Tucker* [1950], who showed suggestive correlations between wave groups and low-frequency motions. In both cases the infragravity wave heights were about 10% of the incident wave heights.

Weak nonlinear interactions between first-order free waves (sea and swell) of nearly equal frequency is one possible mechanism of generating infragravity waves bound (i.e., phase coupled) to groups of higher-frequency waves [*Biesel*, 1952; *Longuet-Higgins and Stewart*, 1960, 1962; *Hasselmann*, 1962; and others]. Phase coupling between infragravity waves and sea and swell has been observed in 8- to 18-m depths [*Hasselmann et al.*, 1963; *Meadows et al.*, 1982; *Elgar and Guza*, 1985; *Elgar et al.*, 1989]. Biphases of pressure in depths of 8 m [*Elgar et al.*, 1989], 11 m [*Hasselmann et al.*, 1963], and 18 m [*Elgar and Guza*, 1985] show that interactions between waves near the peak frequency of the spectrum drive infragravity motions with a depression of sea level under the largest waves in a group, consistent with bound wave theory for nearly collinear waves. These observations show that bound waves are detectable, but quantitative comparisons of predicted bound wave and observed infragravity energy levels are surprisingly limited. Using two 70-min-long records of energetic wave conditions in 40-m depth, *Sand* [1982*b*] found very good agreement (predictions within about 5% of the total observed infragravity energy) at a site in the North Sea a few hundred kilometers distant from the coast, with the assumption that the bound waves and forcing waves (sea and swell) were collinear. However, other observations suggest that free infragravity waves, as well as bound waves, are important.

Paper number 92JC00270.
0148-0227/92/92JC-00270$05.00

Following the early observations by *Munk* [1949] and *Tucker* [1950] suggesting that the seaward propagating infragravity wave amplitude was at least as large as the amplitudes of the shoreward propagating bound wave, *Longuet-Higgins and Stewart* [1962] speculated that the incoming bound wave somehow reflects from the shoreline and radiates seaward as a free wave. Numerical models [*Symonds et al.*, 1982] suggest that slow modulation of the breakpoint position at the group frequency results in long-wave radiation seaward from the breakpoint, but laboratory results are inconclusive. *Kostense* [1984] measured the amplitudes of infragravity waves in shallow water induced by wave grouping in a long wave channel with a plane beach at one end. The observed and theoretical bound wave amplitudes agreed, but there were significant differences between the experimentally observed outgoing free wave amplitudes and those predicted by *Symonds et al.* [1982]. *Kostense* [1984] attributed these differences to assumptions made in the *Symonds et al.* model which failed to include the incoming bound wave and assumed complete reflection at the shoreline, both assumptions affect the outgoing wave amplitude. However, similar laboratory experiments by *Mansard and Barthel* [1984] do not appear to show the presence of breakpoint-forced outgoing waves. It is unclear how, or if, shoreward propagating bound wave energy is reflected from very shallow water.

Another generation mechanism of infragravity motions has been proposed by *Gallagher* [1971], who showed theoretically that certain directional distributions of the incident wave field can resonantly excite edge waves (free waves trapped in shallow water by reflection and refraction). Laboratory results confirm that these directional distributions indeed yield elevated infragravity energy levels [*Bowen and Guza*, 1978]. Recent observations with arrays of flow meters in very shallow depths (<3 m) show that infragravity energy levels increase substantially near the shoreline and include a significant contribution from edge waves [*Huntley et al.*, 1981; *Oltman-Shay and Guza*, 1987; *Howd et al.*, 1991]. Roughly 30–50% of the run-up variance at infragravity frequencies is estimated to be contributed by edge waves with mode numbers ≤ 2 [*Oltman-Shay and Guza*, 1987]. While the presence of low-mode edge waves can explain the observed energy in the longshore velocity field, low-mode edge waves alone cannot describe the observed cross-shore velocity field.

Other waves affecting the cross-shore velocity much more than the longshore, such as high-mode edge waves and/or leaky waves, are clearly present in field data from surf zones.

Although the generation mechanism of free infragravity waves is unclear, bound waves, edge waves, and reflections of $O(1)$ at the shoreline (producing standing waves) have been detected in many field observations in very shallow water ($\lesssim 3$ m) within a few hundred meters of the shoreline [*Suhayda*, 1974; *Huntley*, 1976; *Sasaki et al.*, 1976; *Sasaki and Horikawa*, 1978; *Holman*, 1981; *Huntley et al.*, 1981; *Guza et al.*, 1984; *Huntley and Kim*, 1984; *Guza and Thornton*, 1985; *Elgar and Guza*, 1985; *List*, 1986; and others]. Preliminary results from several hours of data from an array further offshore (8-m depth, about 1 km from shore) suggests that high-mode edge waves (mode number ≥ 3) may sometimes contribute significantly to (or dominate) the infragravity wave field well outside the surf zone where low-mode edge waves are not energetic [*Oltman-Shay et al.*, 1989; *Elgar et al.*, 1989; J. Oltman-Shay, personal communication, 1990]. However, *Sand*'s [1982*b*] results (based on the assumption of unidirectional waves) suggest that bound waves dominate in 40 m depth. In addition, directional spectra measured in 12.5-m depth, approximately 6 km off the New Jersey coast, show the infragravity waves (15- to 85-s periods) to be propagating onshore in the same direction as the swell (15-s period). Seaward propagating leaky waves or longshore propagating edge waves were not detectable [*Goodman et al.*, 1989].

The relative importance of bound waves, high-mode edge waves, and leaky waves, as a function of position on the continental shelf and other variables, is not known. Here we assess the relative importance of bound waves well outside the surf zone in the depth range 8–13 m (0.4–0.8 km offshore), where bound wave theory has been applied with qualitative success [*Hasselmann et al.*, 1963]. This data set, which also includes sensors in 4.5- and 7.0-m depths, consists of 2 years of observations from Barbers Point, Hawaii, and Imperial Beach, California. Several days of data from 183-m depth, 10 km offshore on the continental shelf near Point Conception, California, are also considered.

Bound wave theory is reviewed in section 2. Examples are given which illustrate the strong dependence of bound wave energy levels on directional spreading, water depth, and other parameters. The field sites and data sets are described in section 3. Bound wave model-data comparisons are presented in section 4. We conclude that bound waves contribute less than half of the observed infragravity energy in 8- to 13-m depths, and a much smaller fraction in 183-m depth. The remainder is free (either leaky or edge) wave energy. In section 5 we show that only a small amount (at most 10%) of the free wave energy in 8- to 13-m depth reaches the gage in 183-m depth. Most of the free infragravity energy in 8- to 13-m depth is refractively trapped edge waves. The results are summarized in section 6.

2. BOUND WAVE THEORY REVIEW

Predictions of infragravity bound waves in constant depth are obtained by expanding the inviscid, incompressible, irrotational wave equations and boundary conditions, by the method of Stokes, to second order in the wave slope [*Biesel*, 1952; *Longuet-Higgins and Stewart*, 1960, 1962, 1964; *Hasselmann*, 1962; and others]. At lowest order the sea surface elevation is assumed to be a linear sum of free waves (sea and swell),

$$\eta^{(1)} = \sum_{n=n_{lo}}^{n_{hi}} \sum_{q=1}^{n_\theta} A_{n,q} \sin(k_n x \cos\theta_q + k_n y \sin\theta_q - \omega_n t + \phi_{n,q}) \cdot (\delta\omega\delta\theta)^{1/2}, \quad (1)$$

where $\omega_n^2 = g k_n \tanh k_n h$, h is the depth, (x, y) are the horizontal coordinates, and $\delta\omega$, $\delta\theta$ are the frequency and directional resolution, respectively. $A_{n,q}$ and $\phi_{n,q}$ are the first-order free wave amplitude density and phase, respectively, of waves with radian frequency $\omega_n (= n\,\delta\omega)$, vector wavenumber $\vec{k}_n (k_n = |\vec{k}_n|)$, and propagation direction θ_q. The lowest and highest free wave (sea and swell) frequencies are $n_{lo}\delta\omega$ and $n_{hi}\delta\omega$, respectively, and $n_\theta = 360/\delta\theta$ is the number of directional bands at each frequency.

The second-order (bound wave) sea surface elevation with only the difference frequencies retained are

$$\eta^{(2)}(\omega_j) = \sum_{n=n_{lo}}^{n_{hi}-j} \sum_{q=1}^{n_\theta} \sum_{r=1}^{n_\theta} {}_eC A_{n,q} A_{n+j,r} \cdot \cos[\Delta k x \cos\theta_b + \Delta k y \sin\theta_b - \omega_j t + \Delta\phi]\delta\omega\delta\theta, \quad (2)$$

where the bound wave frequency $\omega_j = \omega_{n+j} - \omega_n$, the bound wave vector wavenumber $\vec{\Delta k} = \vec{k}_{n+j,r} - \vec{k}_{n,q} = (\Delta k \cos\theta_b, \Delta k \sin\theta_b)$, $\Delta k = |\vec{\Delta k}|$, and $\Delta\phi = \phi_{n+j,r} - \phi_{n,q}$ is the bound wave phase. The bound wave sea surface elevation coupling coefficient ${}_eC$ is a function of the free wave frequencies ω_{n+j}, ω_n and the angular difference $\Delta\theta = \theta_{n+j,r} - \theta_{n,q}$. Note that the bound wave propagation direction θ_b is determined from the vector difference $\vec{\Delta k}$ and is not equal to $\Delta\theta$.

Assuming that the first-order free waves have random phases, the infragravity bound wave sea surface elevation frequency spectrum ${}_eS^{(2)}(\omega_j)$ is [*Hasselmann*, 1962]

$${}_eS^{(2)}(\omega_j) = 2\delta\omega \sum_{n=n_{lo}}^{n_{hi}-j} \sum_{q=1}^{n_\theta} \sum_{r=1}^{n_\theta} {}_eC^2 \cdot S^{(1)}(\omega_n, \theta_q) S^{(1)}(\omega_{n+j}, \theta_r) \delta\theta^2, \quad (3)$$

where the free wave (sea and swell) frequency-directional spectrum is $S^{(1)}(\omega_n, \theta_q)$ and the bound wave energy at frequency ω_j has been summed over all the infragravity wave directions θ_b. The bound wave pressure spectrum is given by equation (3) with ${}_eC$ replaced by ${}_pC$, the bound wave pressure coupling coefficient. Frequency-directional wavenumber spectra of bound waves are obtained with separate summations over the free wave components contributing to specific infragravity frequencies and wavenumbers. The bound wave sea surface elevation spectrum ${}_eS^{(2)}$ is related to the smoothed instantaneous wave energy history (SIWEH) spectrum [*Funke and Mansard*, 1979; *Sand*, 1982b]. The SIWEH spectrum describes the grouping structure of the sea and swell wave field but lacks the coupling coefficient ${}_eC$ theoretically relating the amplitudes of groups and bound waves, and can thus only very qualitatively mimic the physics of bound wave theory.

The coupling coefficients ${}_eC$ and ${}_pC$ (at vertical distance z measured from the sea surface) are given by [*Hasselmann*, 1962; *Sand*, 1982*a*]

$$ {}_{\epsilon}C = -\frac{gk_n k_{n+j}\cos\Delta\theta}{2\omega_n\omega_{n+j}} - \frac{\omega_n\omega_{n+j}}{2g} + \frac{(\omega_n^2+\omega_{n+j}^2)}{2g} $$

$$ - \frac{g\omega_j}{[g\Delta k\tanh(\Delta kh)-\omega_j^2]\omega_n\omega_{n+j}} \left\{ \omega_j \left[\left[\frac{\omega_n\omega_{n+j}}{g} \right]^2 + k_n k_{n+j}\cos\Delta\theta \right] - \frac{1}{2}\left[\frac{\omega_n k_{n+j}^2}{\cosh^2(k_{n+j}h)} - \frac{\omega_{n+j}k_n^2}{\cosh^2(k_n h)} \right] \right\} \quad (4a) $$

and

$$ {}_{p}C = -\frac{gk_n k_{n+j}\cos\Delta\theta\cosh[k_n(z+h)]\cosh[k_{n+j}(z+h)]}{2\omega_n\omega_{n+j}\cosh(k_n h)\cosh(k_{n+j}h)} - \frac{gk_n k_{n+j}\sinh[k_n(z+h)]\sinh[k_{n+j}(z+h)]}{2\omega_n\omega_{n+j}\cosh(k_n h)\cosh(k_{n+j}h)} $$

$$ - \frac{g\omega_j\cosh[\Delta k(z+h)]}{[g\Delta k\tanh(\Delta kh)-\omega_j^2]\omega_n\omega_{n+j}\cosh(\Delta kh)} \left\{ \omega_j \left[\left[\frac{\omega_n\omega_{n+j}}{g} \right]^2 + k_n k_{n+j}\cos\Delta\theta \right] - \frac{1}{2}\left[\frac{\omega_n k_{n+j}^2}{\cosh^2(k_{n+j}h)} - \frac{\omega_{n+j}k_n^2}{\cosh^2(k_n h)} \right] \right\}, \quad (4b) $$

where the sign of the coupling coefficient relates the phases of the bound waves and the free wave groups. When the interacting free waves are collinear ($\Delta\theta = 0°$), the magnitude of the sea surface elevation coupling coefficient $|{}_{\epsilon}C|$ is larger than the bottom ($z = -h$) pressure coupling coefficient $|{}_{p}C|$ in all depths. However, in water shallow for the sea and swell, ($\omega_n^2 h/g \ll 1$) $|{}_{\epsilon}C| \sim |{}_{p}C|$, whereas in deep water, $|{}_{\epsilon}C| \gg |{}_{p}C|$ (Figure 1*a*). For directionally spread ($\Delta\theta \neq 0°$) incident waves there are intermediate depths and incident wave frequencies where $|{}_{p}C|$ is slightly larger than $|{}_{\epsilon}C|$ (Figure 1*b*, $\Delta\theta = 20°$), and the bound wave pressure fluctuations at the seafloor are actually larger than an unattenuated hydrostatic response to infragravity sea surface displacements. The bound wave response varies somewhat with changes in the ratio of bound to free wave frequency (ω_j/ω_n; Figure 1*a*), and strongly as a function of the angular spread, depth, and free wave frequency (Figure 1*b*). In shallow water (for the sea and swell) the magnitude of the coupling coefficients are largest when the interacting waves are collinear ($\Delta\theta = 0°$), and bound waves forced by even slightly directionally spread seas are theoretically significantly smaller than with unidirectional seas (compare $\Delta\theta = 0°$ with $\Delta\theta = 10°$ in Figures 1*b* and 2*a* and Table 1). In contrast, when the sea and swell waves are in deep water, the sea surface elevation coupling coefficient has the largest magnitude for large angular spread (Figure 1*b*), and free waves with a directionally broad spectrum may force more bound wave energy at the sea surface than is forced by a relatively narrower spectrum (Figures 2*c* and 2*d* and Table 1).

For collinear free waves, the bound infragravity wave is 180° out of phase with the free wave groups (i.e., ${}_{\epsilon}C$ and ${}_{p}C$ are negative) and the infragravity wave trough occurs beneath the high waves in the group [*Longuet-Higgins and Stewart*, 1962]. For moderately large $\Delta\theta$(≥30° in deep water; Figure 1*b*), the sea surface elevation coupling coefficient changes sign and the analogous phase is 0°. With increasingly large $\Delta\theta$, both groups and bound waves have progressively shorter spatial scales in both horizontal directions. When the angular spread between interacting free waves of about the same frequency is very large ($\Delta\theta > 90°$), the bound wavenumber is

$$ |\vec{\Delta k}| = |\vec{k}_{n+j,r} - \vec{k}_{n,q}| > \sqrt{2}\,|\vec{k}_{n+j,r}| \quad (5) $$

and the infragravity bound wave is shorter than the forcing free waves. These bound waves are coupled to the "checkerboard" pattern of short-crested waves rather than the "group" structure of long-crested waves. The bound wave crest occurs under maxima in the checkerboard.

It does not seem to have been previously noted that with very broad directional distributions in deep water, these short-wavelength waves can theoretically dominate the infragravity bound wave field at the sea surface, owing to the maximum of ${}_{\epsilon}C$ at very large $\Delta\theta$. They will not, however, penetrate deeply into the water column. These short-wavelength, low-frequency waves are generated by the same interacting waves (i.e., directionally opposing wave trains of nearly equal frequencies) that generate the long-wavelength, high-frequency motions that dominate the pressure spectrum on the seafloor in deep water and excite microseisms [*Longuet-Higgins*, 1950]. In very deep water, O(5000 m), the longest infragravity bound waves, driven by collinear interactions, are short [$\Delta k = (\omega_{n+j}^2 - \omega_n^2)/g$] compared with the water depth, attenuation at the seafloor is extreme, and the bottom pressure field is dominated by free infragravity waves [wavenumber $(\omega_{n+j} - \omega_n)^2/g$] radiated from coastlines with energetic sea and swell [*Webb et al.*, 1991]. The most energetic free infragravity waves observed in the deep Pacific [*Webb et al.*, 1991] have variance of about 0.06 cm^2. However, at the sea surface the predicted bound wave variance is ~0.2 cm^2 for energetic (variance ~10^4 cm^2) sea and swell (Table 1). Thus infragravity bound wave energy levels might be comparable to (or larger than) free infragravity waves at the sea surface in the deep ocean, even though free waves dominate the bottom pressure.

As nearly collinear first-order free waves (sea and swell) enter very shallow water, near-resonances occur because the sea and swell group velocity approaches the phase velocity of free infragravity waves. In shallow water, ${}_{\epsilon}C^2$ and ${}_{p}C^2$ become very large for small $\Delta\theta$ (Figure 1), the assumption (of bound wave theory) that predicted bound waves have much smaller amplitudes than the first-order free waves is violated (Figure 3*a*), and qualitative results at best can be expected [*Longuet-Higgins and Stewart*, 1964]. Note that the depth at which bound wave spectral density exceeds the first-order free wave density depends on both the first-order wave amplitudes and frequencies. If the swell energy in Figure 3*a* were reduced by a factor of 10, the predicted bound wave energy would decrease by 10^2 (equation (3)). The shallow water limit of applicability for bound wave theory is not well understood.

For simplicity, consider the sea surface elevation coupling coefficient for collinear free plane waves, with both the free and bound waves in shallow water; to $O(kh)^2$,

$$ {}_{\epsilon}C(\text{shallow}) = -\frac{3}{2}\frac{1}{h^3 k_n k_{n+j}} = -\frac{3}{2}\frac{g}{h^2(\omega_n^2 + \omega_n\omega_j)} \quad (6) $$

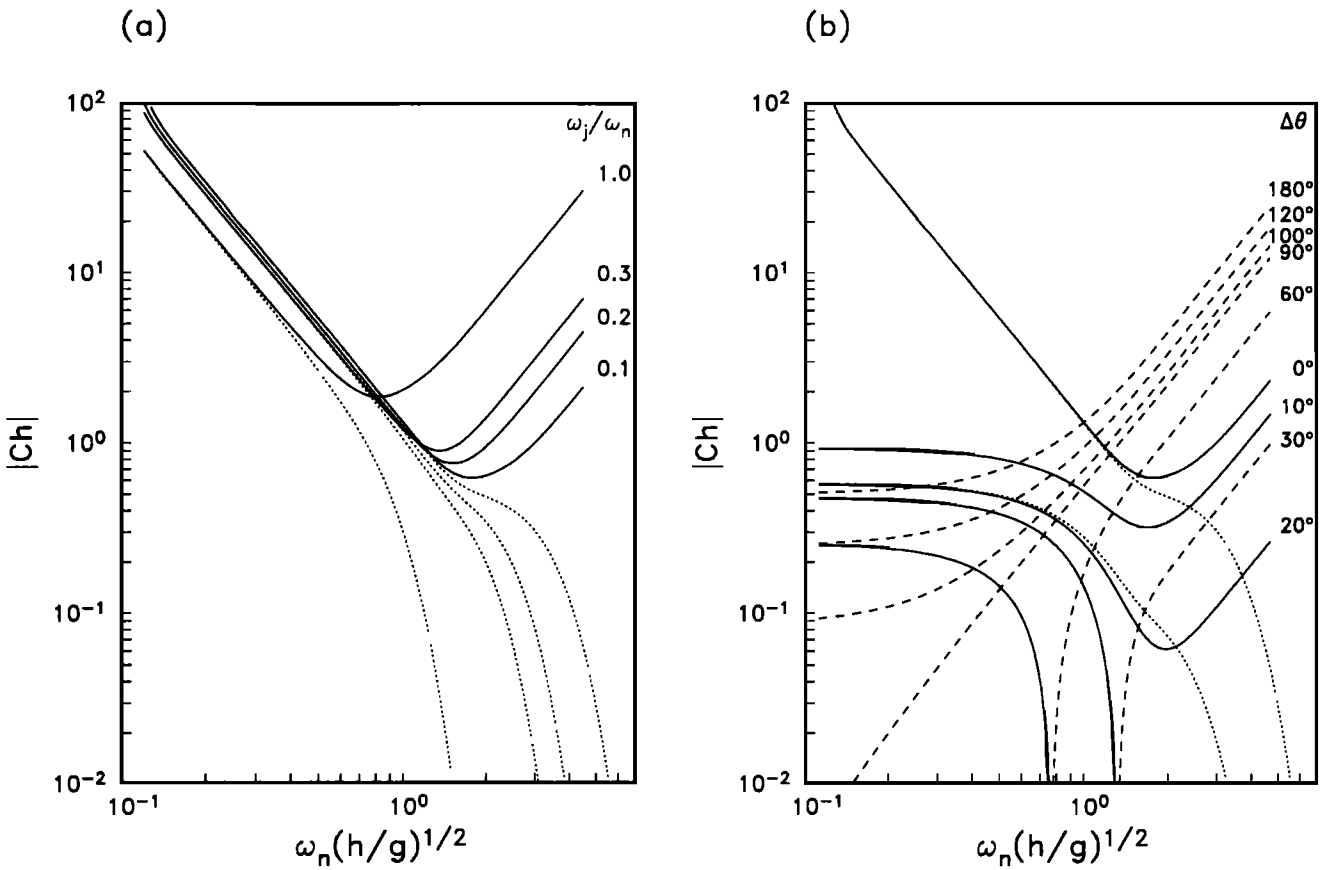

Fig. 1. The nondimensional (note the factor of h) bound wave sea surface elevation coupling coefficient ($|_eCh|$, solid and dashed lines) and bottom ($z=-h$) pressure coupling coefficient ($|_pCh|$, dotted lines) as a function of the first-order free wave radian frequency ω_n, bound wave radian frequency ω_j, depth h, angular separation $\Delta\theta$, and ratio ω_j/ω_n [after *Ottesen Hansen*, 1978; *Sand*, 1982*a*]. (*a*) Various values of ω_j/ω_n and constant $\Delta\theta=0$. (*b*) Various values of $\Delta\theta$ and constant $\omega_j/\omega_n=0.1$. Solid and dotted lines indicate negative values of $_eC$ and $_pC$, respectively, and dashed lines are for positive values of $_eC$.

and the ratio of bound to free wave energy is approximately proportional to Ur^2, where $Ur=(a/h)/(kh)^2$ is the Ursell number and a and k are characteristic free wave amplitude and wavenumber, respectively. Thus bound wave energy in shallow water increases rapidly with decreasing first-order free wave frequencies and decreasing depth. As shown in Figure 3, given equally energetic unidirectional narrow banded swell (O(0.07 Hz)) and sea (O(0.2 Hz)) in the same (10 m) depth, the swell will force about 10^2 times more bound wave energy below 0.04 Hz than the sea.

Nelson et al. [1988] compared infragravity wave heights (H^{obs}) measured in 12 m with sea and swell wave heights (H_{SS}) and frequencies (ω_{SS}) measured in 50 m depth and developed an empirical equation which can be written $H^{obs}\sim(H_{SS}/\omega_{SS})^{1.77}$, a trend in qualitative agreement with the shallow water limit of bound wave theory (bound wave height $H^{bnd}\sim(H_{SS}/\omega_{SS})^2$ from equations (2), (3), and (6); see also *Medina* [1990]). In 21-m depth, *Middleton et al.* [1987] noted a similar dependence of the infragravity energy on the sea and swell frequencies. Infragravity energy increased when swell (11–14 s) energy increased, but not with increases in shorter-period (≤10 s) waves. A dependence of the infragravity energy levels on the incident sea and swell frequencies has also been observed in the surf zone [*Goda*, 1975; *Holman and Sallenger*, 1985].

In deep water ($kh\gg1$) for collinear free waves,

$$_eC(\text{deep})=-\frac{1}{2}(k_{n+j}-k_n)=-\frac{1}{2g}(\omega_{n+j}+\omega_n)(\omega_{n+j}-\omega_n) \quad (7)$$

and the ratio of bound infragravity to free sea and swell energy is proportional to $(ak)(a\omega_j^2/g)$ where ak is the first-order free wave steepness and ω_j is the bound wave frequency. At a fixed ω_j, $|_eC|$ increases for increasing free wave frequencies (or wavenumber) in deep water, and sea forces more infragravity energy at the surface than is forced by swell of the same height (compare spectra for 200-m depths in Figures 3*a* and 3*b*); the relative response is reversed compared to shallow water. Owing to the relative importance of steep wind waves to infragravity wave generation in deep water, subsurface pressure sensors (which cannot sense short wind waves because of hydrodynamic attenuation) may not provide data suitable for bound wave predictions at the surface. Also in contrast to shallow water, in deep water $|_eC|$ increases with increasing bound wave frequency so the spectrum of bound waves in deep water is generally not white but most energetic at a frequency that roughly corresponds to the width of the free wave spectrum.

3. Field Measurements And Data Processing

Field measurements were made at Barbers Point Harbor, Hawaii, on the southwest side of Oahu; at Imperial Beach, California; and offshore of Point Conception, California. The Barbers

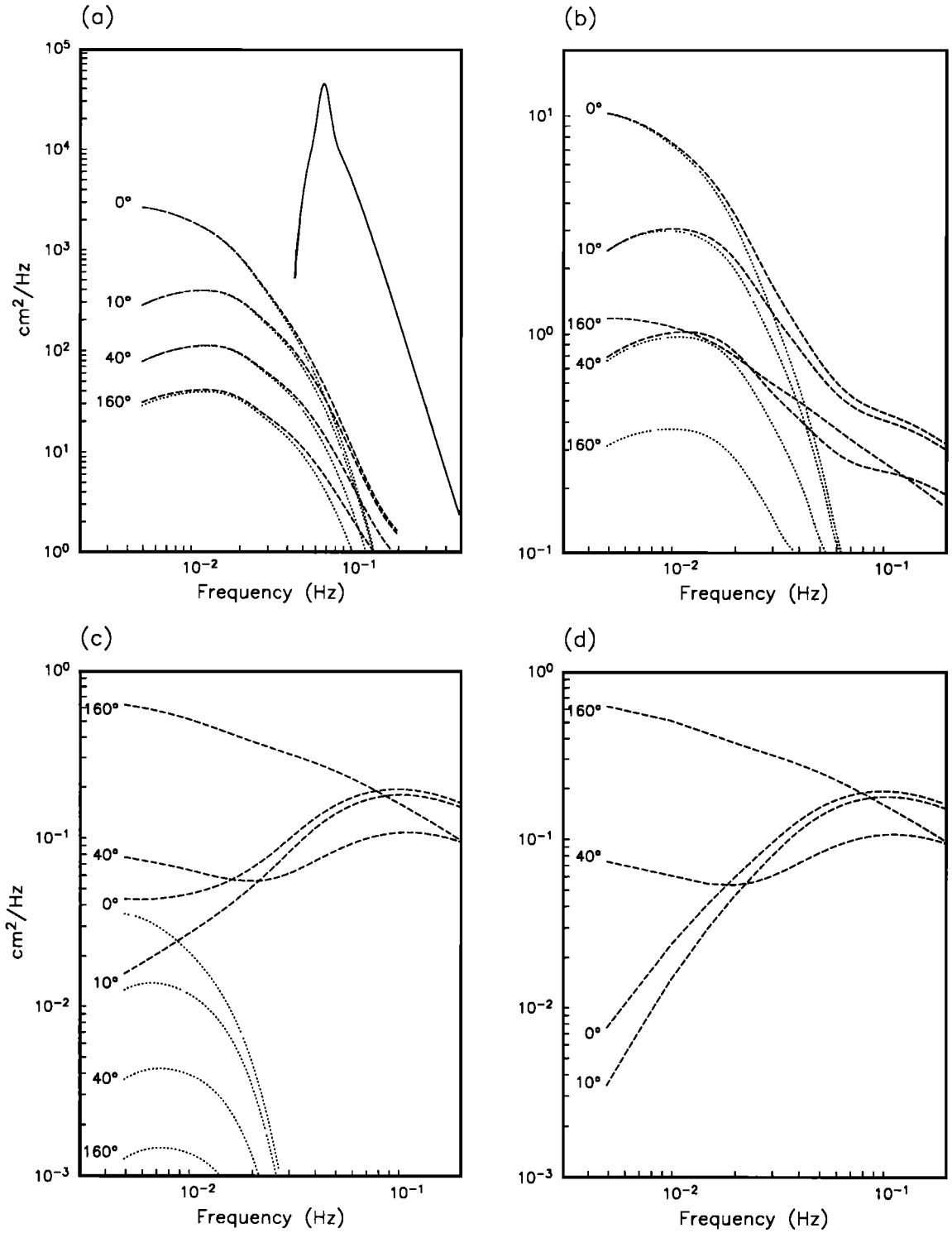

Fig. 2. Bound wave sea surface elevation spectra (dashed lines) and bottom ($z = -h$) pressure (dotted lines) in depths of (*a*) 10 m, (*b*) 40 m, (*c*) 183 m and (*d*) 5000 m forced by the same first-order free wave (solid line, f >0.04 Hz) energy spectrum (Figure 2*a*) and $\cos^d\theta$ directional distribution (all frequency bands have the same directional spread determined by *d*). The full angular widths (degrees) at 50% of the maximum free wave spectral energy density are indicated, and the total sea and swell energy is 10^3 cm^2. The total bound wave sea surface elevation and bottom pressure energy for f <0.04 Hz for the various angular widths and depths are given in Table 1.

Point data were collected between June 1988 and March 1990 as part of a study of oscillations within the 0.37 km^2, 11.6-m-deep harbor basin (Figure 4). Access to the basin is through a 1.3-km-long entrance channel, dredged to a depth of 12.8 m. The coral rock beach slopes rather steeply (~0.04 slope) from the shoreline to 3-m depth, then slopes gradually (~0.01) to the 9-m contour approximately 0.8 km offshore, followed by a steeper (~0.08) slope between the 9-m and 18-m contours, beyond which the depth increases to 180 m within another 0.8 km. We primarily use data from four near-bottom pressure sensors arranged in a 6 m

TABLE 1. Total Bound Wave Sea Surface Elevation and Bottom Pressure Energy for f <0.04 Hz for the Angular Widths and Depths in Figure 2

	Angular Width							
	0°		10°		40°		160°	
Depth,m	Sea Surface Elevation Energy, cm^2	Bottom Pressure Energy, cm^2	Sea Surface Elevation Energy, cm^2	Bottom Pressure Energy, cm^2	Sea Surface Elevation Energy, cm^2	Bottom Pressure Energy, cm^2	Sea Surface Elevation Energy, cm^2	Bottom Pressure Energy, cm^2
10	41.0	40.6	10.2	10.0	3.1	3.0	1.1	1.1
40	0.16	0.15	0.075	0.066	0.028	0.024	0.031	9.0×10^{-3}
183	0.0031	3.7×10^{-4}	0.0024	1.8×10^{-4}	0.0025	6.2×10^{-5}	0.016	2.2×10^{-5}
5000	0.0027	$<10^{-7}$	0.0020	$<10^{-7}$	0.0024	$<10^{-7}$	0.016	$<10^{-7}$

x 6 m square slope array located outside the harbor just north of the entrance channel in 8.7 m mean depth. Data were also acquired from bottom-mounted pressure sensors in 7.0- and 4.5-m depth (Figure 4). The tidal range at Barbers Point was approximately 0.9 m.

Imperial Beach, located just north of the California-Mexico border, is a west-facing sandy beach with a relatively straight shoreline and plane beach slope (~0.025). The Imperial Beach data set is from a 6 m x 6 m slope array located approximately 0.4 km offshore in about 11.5-m mean depth, collected from December 1989 to August 1991. The tidal range was approximately 2.4 m. At Barbers Point and Imperial Beach 2.3-hour-long records were obtained at a 1 Hz sample rate, four times a day. There were 557 and 2301 records at Barbers Point and Imperial Beach, respectively.

Offshore data were obtained with a Baylor wave staff mounted on the Chevron oil platform *Hermosa* in 183-m depth approximately 10 km from shore between Point Arguello and Point Conception, California. Ten time series each of 34-min duration and sampled at 2 Hz were analyzed.

The energy density in the infragravity band can be 10^2 times lower than in the sea and swell band (e.g., Figure 6), and the quality of these relatively low signals could be degraded by nonlinearity in either the basic sensor (either pressure or wave staff) or "flow noise" due to disturbance of the flow by a pressure sensor. However, infragravity spectra measured by pressure sensors within a slope array were similar, as would probably not be the case if sensor nonlinearity or flow noise were dominant.

Fourier coefficients of pressure and sea surface elevation were calculated for overlapped 1024-s records which were first quadratically detrended to suppress tidal and other low-frequency motions with periods greater than the record length, and tapered with a triangular window to reduce spectral leakage. The Fourier coefficients of pressure at sea and swell frequencies were converted to sea surface elevation with linear theory. Smoothed power spectra for each 2.3-hour record were obtained by averaging over 1024-s segments and merging over five frequency bands, resulting in a spectral bandwidth of 4.88×10^{-3} Hz with 100–200 degrees of freedom (DOF) at Barbers Point and Imperial Beach and ~30 DOF at Point Conception. Frequency-directional

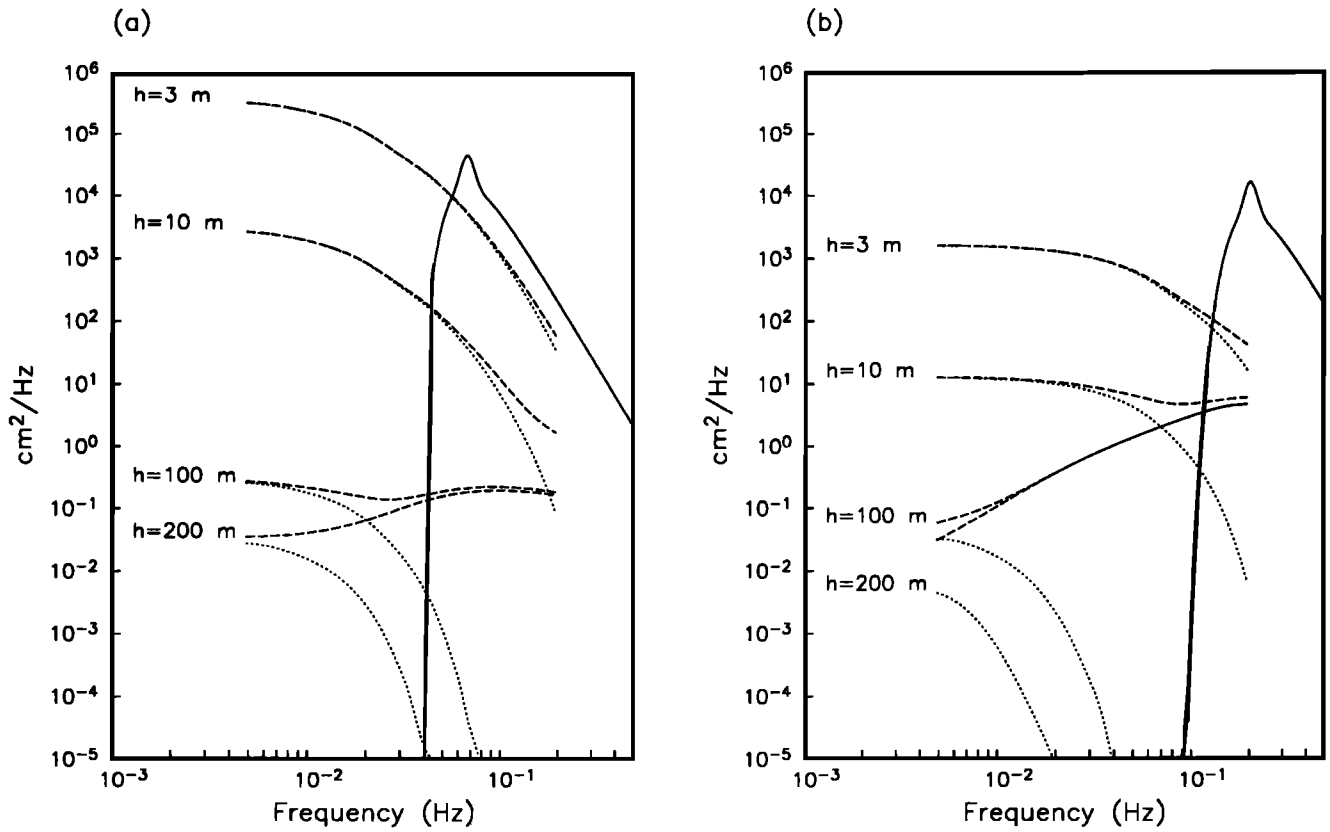

Fig. 3. Bound wave sea surface elevation spectra (dashed lines) and bottom pressure spectra (dotted lines) forced by unidirectional (*a*) swell (~0.07 Hz peak) and (*b*) sea (~0.2 Hz peak) of equal total energy (10^3 cm^2, solid line) in depths h = 3, 10, 100, and 200 m.

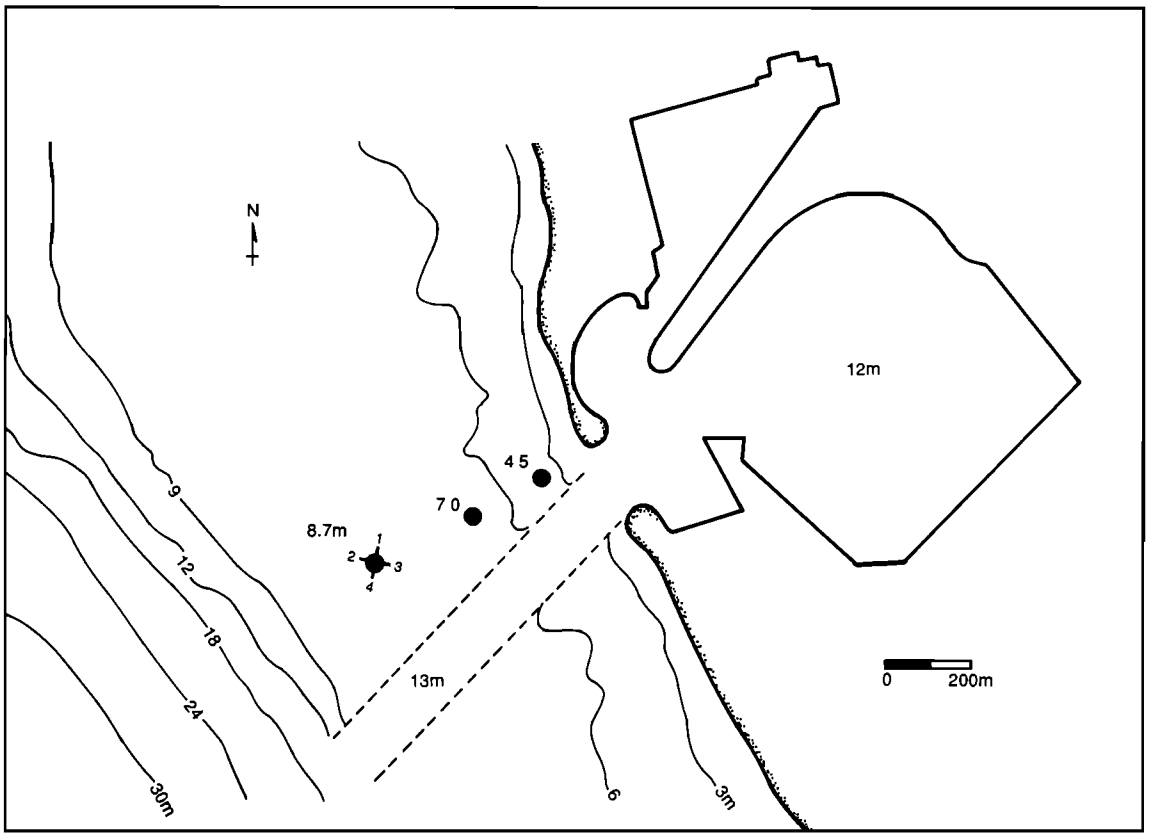

Fig. 4. Instrument positions and depths at Barbers Point. Solid dots are single point pressure sensors, and the solid dot with cross is a 6 m x 6 m array of four pressure sensors.

spectra were crudely estimated at Imperial Beach and Barbers Point. The mean direction $\theta_0(f)$ and spreading parameter $s(f)$ in the widely used $\cos^{2s(f)}[\theta(f)-\theta_0(f)]$ parametric directional distribution were obtained from the slope array cross spectra (see appendix).

4. Bound Wave Predictions And Observations

The sea surface elevation and pressure variance below 0.04 Hz were defined as infragravity wave energy (${}_eE^{obs}$ and ${}_pE^{obs}$, respectively), while the sea surface elevation variance between 0.04 and 0.25 Hz was assumed to be free sea and swell wave energy (E_{SS}). The fixed cutoff frequency of 0.04 Hz between infragravity and sea and swell waves was selected so that very little energy of long swell was included in the infragravity band. A basic question that is addressed is whether bound waves dominate the total energy in the infragravity band. If the cutoff frequency is high enough so that significant amounts of swell energy fall in the defined infragravity band, then the bound wave prediction will be much lower than observed, and the result will necessarily be that bound waves are insignificant. The 0.04-Hz cutoff frequency was based on comparisons of many predicted bound wave and observed spectra. As illustrated in Figures 6 and 12 (to be discussed later) a spectral minimum was nearly always observed at a frequency near (or above) 0.04 Hz. At frequencies higher than this minimum, the observed power level rises dramatically and the predicted bound wave energy levels are much lower than observed owing to the importance of swell. Obviously, the value of a fixed cutoff would vary according to the wave climate at a particular site; 0.04 Hz is appropriate for the present observations in the Pacific Ocean.

The frequency band studied here (f <0.04 Hz) does not necessarily contain most of the energy forced by nonlinear difference interactions. For example, in 100- and 200-m depths in Figure 3 there is much more forced energy at the sea surface in the band 0.04 to 0.20 Hz than below 0.04 Hz, although the 0.04 to 0.20-Hz forced energy is much lower than the free swell energy in this band. Thus we attempt not to identify all the energy forced by difference frequency interactions, but rather to assess whether forced waves dominate a low-frequency band where free waves might be negligible. The relatively small amount of bound wave energy above 0.04 Hz (Figures 6 and 12) included as part of the free wave (forcing) spectrum at swell frequencies does not cause significant errors in bound wave predictions below 0.04 Hz. There are cases (not shown) in which the spectrum above 0.04 Hz consists of a swell peak at f_p and an additional peak at $2f_p$. Bispectral analysis [e.g., *Elgar and Guza*, 1985] shows the energy at $2f_p$ to be phase-coupled bound harmonics driven by sum interactions, and not free wave energy as assumed in the calculation of infragravity bound wave energy. This is of little consequence here, however, because in shallow water the swell peak provides virtually all the bound infragravity wave forcing (Figures 1 and 3) and the predictions are insensitive to harmonic energy.

Similar to previous results, the observed infragravity wave heights (H^{obs}) and sea and swell significant heights (H_{SS}) at both Barbers Point (8.7-m depth) and Imperial Beach (10.2–12.7 m) are significantly correlated (Table 2). (Significant heights are defined as 4σ, where σ^2 is the band-passed variance in each frequency range.) H^{obs} and H_{SS} are also highly correlated in shallower depths (4.5 m and 7.0 m) at Barbers Point and deeper (183 m) water at Point Conception. The slope of the best fit linear regression line through the data points (H^{obs},H_{SS}) ~O(0.1) in

TABLE 2. Simple Relationships Between H^{obs} and H_{SS}

Site	Depth, m	Slope	Corr
T.P./S.B	swash	1.00	0.78
T.P./S.B.	0.0 – 1.0	0.37	0.54
T.P./S.B.	1.0 – 2.0	0.32	0.86
B.P.	4.5	0.20	0.96
B.P.	7.0	0.17	0.90
B.P.	8.2 – 9.1	0.14	0.92
I.B.	10.2 – 11.0	0.13	0.87
I.B.	11.1 – 11.8	0.13	0.88
I.B.	11.9 – 12.7	0.13	0.85
I.B.	10.3 – 12.7	0.13	0.86
North Sea	40.0	0.04	---
P.C.	183	0.03	0.97

Slope is the slope of the linear regression line between H^{obs} and H_{SS}, and Corr is the correlation. All correlations shown are significant. Sites in the present study are Barbers Point (B.P.), Imperial Beach (I.B.), and Point Conception (P.C.). Similarly processed data from Torrey Pines (T.P.) and Santa Barbara (S.B.) are included for comparison; H_{SS} in these cases was measured in 7- to 10-m depth [*Guza and Thornton*, 1985]. *Sand* [1982*b*] had two records, each 1 hour long, from the North Sea.

depths of ~8–13 m is similar to past observations in these depths [e.g., *Munk*, 1949; *Tucker*, 1950], as are the shallower observations at Barbers Point (Table 2, and data from previous studies not shown). Regression line slopes are considerably smaller in both 40-m [*Sand*, 1982*b*] and 183-m depth. Note that bound wave theory does not predict a linear relationship between H^{obs} and H_{SS}; for a free wave field with the shape of the frequency-directional spectrum and depth held constant, and only the total power level varied, $H^{obs} \sim H_{SS}{}^2$.

Wave spectra in ~10-m depth at Imperial Beach and Barbers Point were separated into three groups delineated by the frequency of the maximum spectral level. As shown in Figure 5, for a given total sea and swell energy (E_{SS}), the observed infragravity energy (${}_pE^{obs}$) is clearly larger for swell than for higher frequency [O (0.10 Hz)] wind waves (particularly for energetic events), a trend qualitatively consistent with both bound wave theory (equation (6) and Figure 3) and other observations [*Middleton et al.*, 1987; *Nelson et al.*, 1988]. With similar E_{SS}, E^{obs} in 183-m depth is near 10^{-2} times less than in 10- to 13-m depth (Figure 5*b*).

The observed sea surface elevation spectra above 0.04 Hz (assumed to be free waves) were used to predict (equation (3)) the infragravity bound wave spectra. Figure 6 (and the top panel of Figure 12, discussed later) shows examples of observed and predicted pressure spectra with the sea and swell directional spectra modeled both as $\cos^{2s(f)}[\theta(f) - \theta_0(f)]$ (appendix) and as unidirectional.

Owing to the maximum of the bound wave coupling coefficient C for collinear waves (equation (3), Figure 2*a*), ${}_pE^{bnd}$ is between 2 and 10 times larger with unidirectional free waves (sea and swell) than with directionally spread free waves. Bound waves were also predicted assuming the sea and swell directions were normally distributed about θ_0 with rms directional width given by equation (A2). Differences between the predictions using the $\cos^{2s}$ and Gaussian directional distribution were small. However, the sensitivity of the bound wave model to the directional distribution is strong (Figure 2*a*), so the fundamentally low resolution of the slope array limits the accuracy of bound infragravity wave predictions. Thus the unidirectional wave ${}_pE^{bnd}$ is an upper limit on bound wave model predictions, and ${}_pE^{bnd}$ with a $\cos^{2s}$ distribution is a rough approximation of the effects of directional spreading.

The total observed (f <0.04 Hz) infragravity energy (${}_pE^{obs}$) for the entire Barbers Point and Imperial Beach data sets are compared with bound wave predictions (${}_pE^{bnd}$) with both unidirectional and directionally spread free waves in Figure 7. With directionally spread waves (Figures 7*a* and 7*b*), bound wave theory always predicts less energy than observed (${}_pE^{obs} > {}_pE^{bnd}$). This is not always so with unidirectional free waves (Figures 7*c* and 7*d*), emphasizing the importance of including directional spreading in bound wave calculations.

Both directional and unidirectional models severely underpredict ${}_pE^{obs}$ (${}_pE^{obs} \gg {}_pE^{bnd}$) when ${}_pE^{obs}$ (and sea and swell wave energy; Figure 5) is small. The underprediction when unidirectional sea and swell waves are assumed (which results in an overestimate of ${}_pE^{bnd}$) shows that other types of infragravity motions besides bound waves must sometimes be important in these data sets. The following discussion considers ${}_pE^{bnd}$ predicted with directionally spread waves only, keeping in mind the low resolution of the directional estimates and the sensitivity of bound wave theory to directional spreading.

Much of the scatter in ${}_pE^{obs}$ for fixed ${}_pE^{bnd}$ at Imperial Beach (Figure 7*a*) appears to be correlated with depth changes. The tidal range is 2.4 m at Imperial Beach compared with 0.9 m at Barbers Point, and there is indeed less scatter at Barbers Point (compare Figures 7*a* and 7*b*). The underprediction of ${}_pE^{obs}$ at Imperial Beach is most pronounced at high tide (depth of 12–13 m) with small swell and ${}_pE^{obs}$, and least at low tide with energetic ${}_pE^{obs}$ (spectra for representative extreme cases are shown in Figure 6). The data were binned according to mean water depth and ${}_pE^{obs}$. The ratios (averaged within a bin) of predicted bound wave energy to observed infragravity energy (${}_pE^{bnd}/{}_pE^{obs}$), an estimate of the fraction of the total infragravity energy which is bound in each bin, increase nearly monotonically with increasing ${}_pE^{obs}$ and decreasing depth (Figure 8, Table 3). On average, less than 5% of the energy is estimated to be bound when the depth h is greater than 11.5 m and ${}_pE^{obs}$ <6 cm^2, but more than 20% is bound when h <11 m and ${}_pE^{obs}$ >10^2. The similar values of ${}_pE^{bnd}/{}_pE^{obs}$ in the deepest depth bin at Barbers Point (850–913 cm) and the shallowest Imperial Beach depth bin (1000–1050 cm) are noteworthy given the differences between the sites (i.e., the mainland coast at Imperial Beach compared with the island site near a harbor at Barbers Point). Because ${}_pE^{obs}$ and E_{SS} are strongly correlated (e.g., ${}_pE^{obs}$ ~10 cm^2 when E_{SS} ~1000 cm^2; Figure 5), Figure 8 implies that the fraction of the infragravity energy which is bound (${}_pE^{bnd}/{}_pE^{obs}$) also increases with increasing E_{SS}. This is consistent with the results of *Elgar et al.* [1992] in 8- to 13-m water depth at Duck, North Carolina.

Although the ratios averaged over bins show smooth trends with depth and ${}_pE^{obs}$ (Figure 8), there is considerable scatter of the ratios within a bin (Figure 9). Additional variables besides depth and ${}_pE^{obs}$ apparently influence the fraction of the energy which is bound. For example, certain directional characteristics of the incident wave field may preferentially excite edge waves [*Gallagher*, 1971] and thus reduce the relative importance of bound waves. Note that the tendency for higher ${}_pE^{obs}$ to occur with low-frequency incident swell than with higher-frequency seas of the same energy (Figure 5) is not apparent in the ratio data (Figure 9). Thus the fraction of the energy which is bound does not show a clear trend with the peak frequency of the incident waves.

At the offshore Point Conception site in 183-m depth, there was only a single wave gage, so only unidirectional model predic-

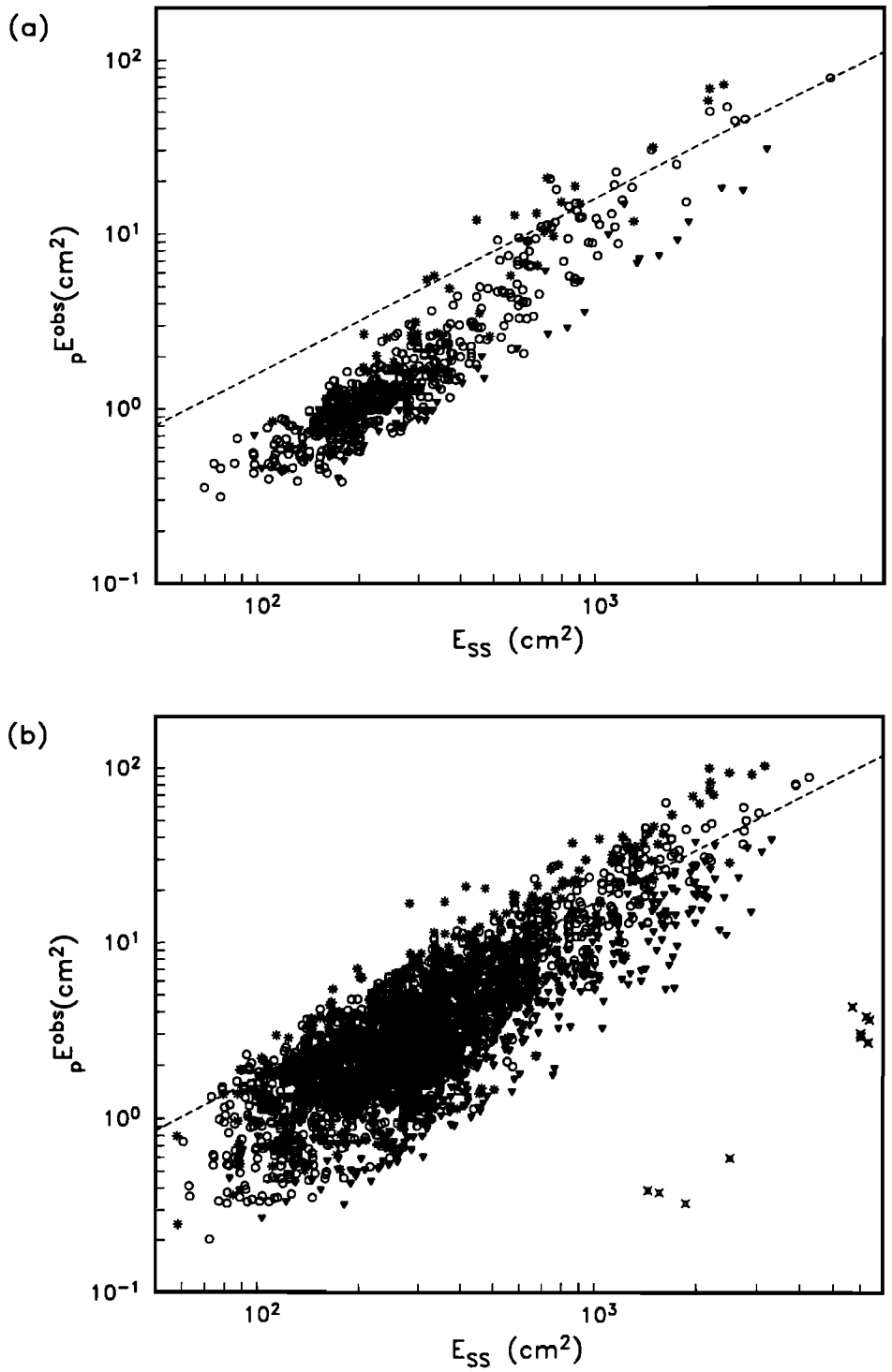

Fig. 5. Observed infragravity ($0.005 < f < 0.04$ Hz) pressure energy ($_pE^{obs}$) versus sea and swell ($0.04 < f < 0.25$ Hz) surface elevation energy (E_{SS}) at (*a*) Barbers Point, 8.2 to 9.1-m depth; (*b*) Imperial Beach, 10.2 to 12.7-m depth. Each plotted point is from a 2.3-hour record. The dashed line is $_pE^{obs} = mE_{SS}$ where m is the slope of the best fit linear regression line between $_pE^{obs}$ and E_{SS}; m = 0.016 (0.017) at Barbers Point (Imperial Beach), and the correlation between $_pE^{obs}$ and E_{SS} is 0.88 (0.83). Peak frequencies (f_p) of each record are $f_p \leq 0.067$ Hz (asterisks), $0.067 < f_p \leq 0.10$ Hz (circles), and $f_p > 0.10$ Hz (triangles). The 10 Point Conception observations (183-m depth) of $_eE^{obs}$ and E_{SS} are shown by crossed squares (Figure 5b).

tions were made (Figure 10). The average (over all 10 records) ratio $_eE^{bnd}/_eE^{obs}$ is 0.047, and accounting for the directional spread in the sea and swell further decreases the energy ratio (unless the directional distribution is unusually broad (Figure 2*c*, Table 1)). The incident sea and swell were energetic at Point Conception, relative to typical conditions at Imperial Beach and Barbers Point. At Point Conception, E_{SS} >1400 cm^2 for all 10 records, and the average E_{SS} = 4400 cm^2 which is comparable to the largest E_{SS} at the shallow sites (Figure 5). Thus on average only a small amount (<5%) of $_eE^{obs}$ is bound in 183-m depth, even with energetic incident waves for which >25% of the energy is bound in shallow water (Figures 5 and 8).

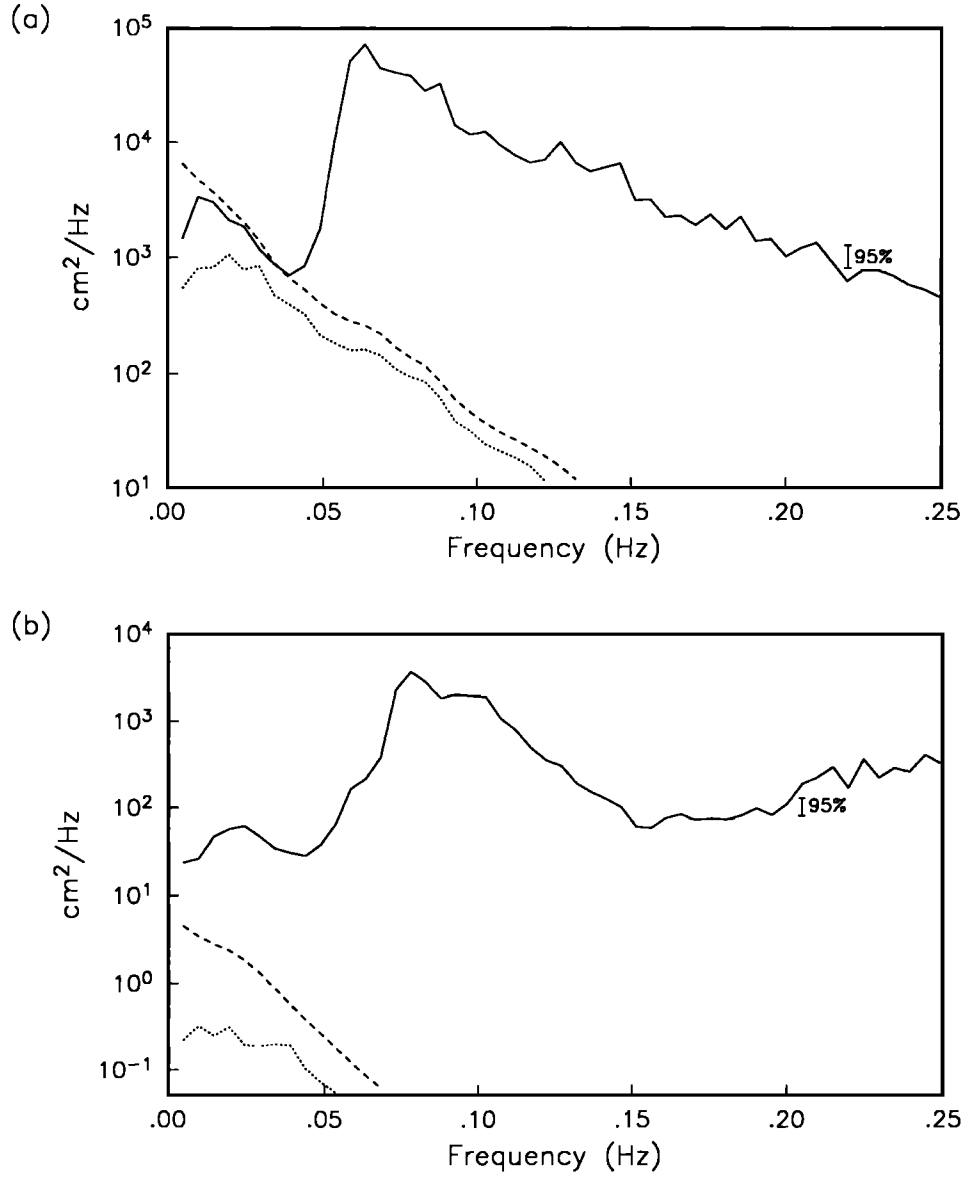

Fig. 6. Observed sea and swell surface elevation spectrum (solid line, $f \geq 0.04$ Hz), observed bottom pressure spectrum (solid line, $f < 0.04$ Hz), unidirectional bound wave model predicted pressure spectrum (dashed line), and directional ($\cos^{2s}$) model predicted pressure spectrum (dotted line) at Imperial Beach. (*a*) March 3, 1991, 0710; h = 10.9 m, E_{SS} = 2239 cm^2, E_p^{obs} = 71 cm^2 and ${}_pE^{bnd}$ = 110 and 28 cm^2 for unidirectional and directional model, respectively. (*b*) November 14, 1990, 0702; h = 12.5 m, E_{SS} = 120 cm^2, ${}_pE^{obs}$ = 1.6 cm^2, and ${}_pE^{bnd}$ = 0.09 and 0.009 cm^2 for unidirectional and directional model, respectively. The ${}_pE^{obs}$ and ${}_pE^{bnd}$ are based on $f < 0.04$ Hz.

5. DISCUSSION

Wave Type Mix

The predicted bound wave energy (E^{bnd}) is less than the observed total infragravity energy (E^{obs}), both in shallow (~10-m depth, Figures 7*a* and 7*b*) and deep (183-m depth, Figure 10) water. The additional observed energy is contributed by free waves (E^{fre}), consisting of both leaky (E^{lky}) and edge (E^{edg}) waves.

$$E^{obs} = E^{bnd} + E^{fre}, \tag{8a}$$

where

$$E^{fre} = E^{lky} + E^{edg}. \tag{8b}$$

By comparing E^{obs} in different depths (h_1 and $h_2, h_1 < h_2$), for similar sea and swell wave energy (E_{SS}), the fraction ($L_{h1,h2}$) of E^{fre} in depth h_1 which radiates to a deeper site (depth h_2) can be estimated. The assumption is made that E_{SS} and h determine the total infragravity energy (and mix of wave types), so observations at the three sites may be combined to form an incoherent array. E^{obs} and the average fraction of E^{obs} estimated to be bound (B),

$$E^{bnd} = BE^{obs} = \langle E^{bnd}/E^{obs} \rangle E^{obs}, \tag{9}$$

are given in Table 4 for the subset of the data with E_{SS} about 1900 cm^2 (H_{SS} ~175 cm). The small number of observations in deep water (Point Conception, Figure 5*b*) is limited to cases of energetic sea and swell.

It follows from the conservation of energy (EC_g = constant, where C_g is the group velocity) that leaky infragravity energy $E^{lky} \sim h^{-1/4}$ for normally incident waves in shallow (relative to the infragravity wavelength) water. On plane parallel contours,

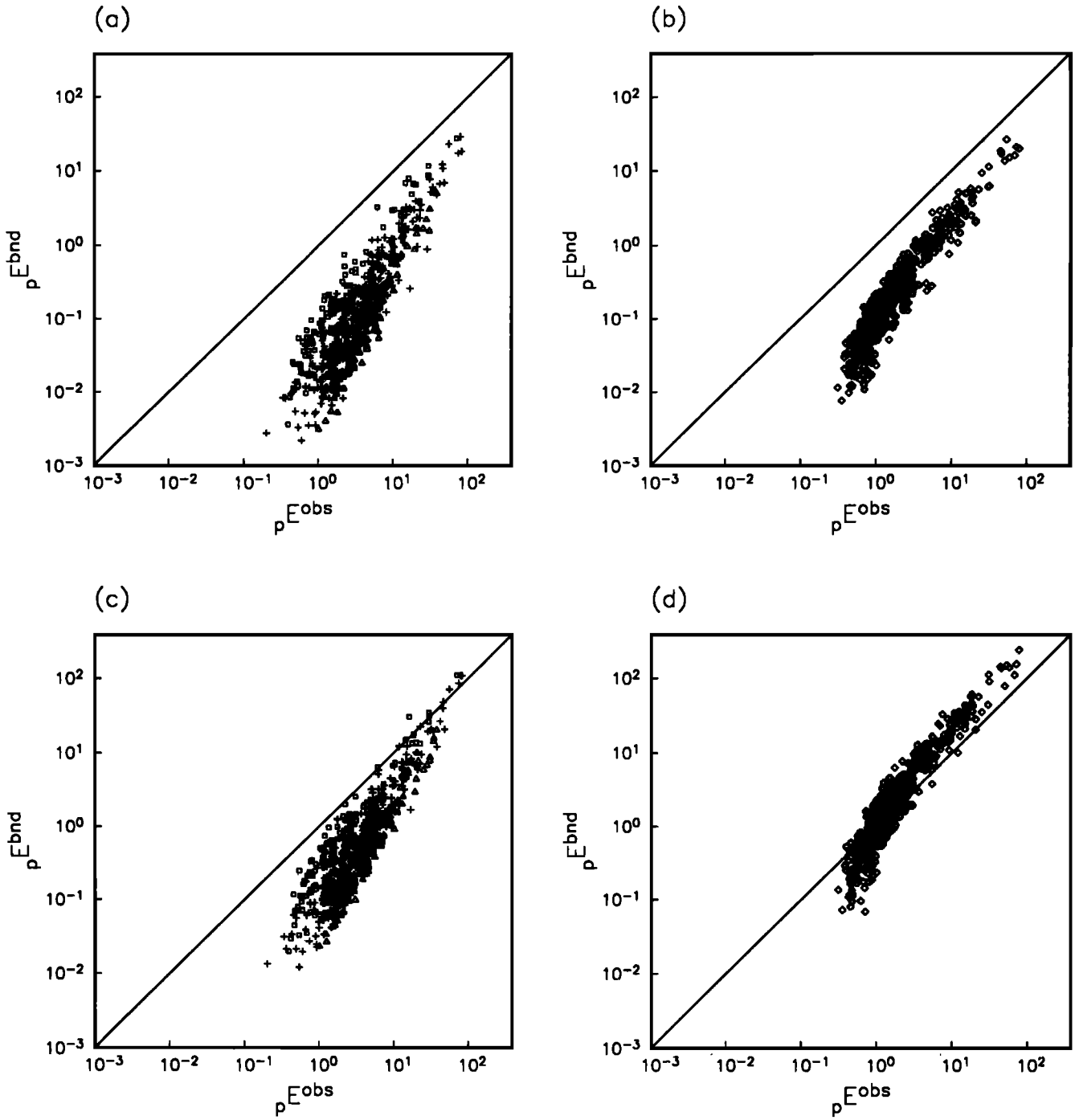

Fig. 7. (*a*, *b*) Directional and (*c*, *d*) unidirectional bound wave model predicted infragravity pressure energy ($_pE^{bnd}$) versus observed infragravity pressure energy ($_pE^{obs}$) at (*a*, *c*) Imperial Beach and (*b*, *d*) Barbers Point. The symbols indicate the mean depth (h) of each record: diamonds, 820 $\leq h \leq$913 cm; squares, 1000 $\leq h \leq$1099 cm; pluses, 1100 $\leq h \leq$1199 cm; triangles, 1200 $\leq h \leq$1300 cm. The solid lines are $_pE^{bnd} = {}_pE^{obs}$. To improve figure clarity, only one fourth of the data points at Imperial Beach are plotted, so about 600 points are shown for each site.

moderate angles of obliquity (<45°) in deep water cause less than 30% deviation from the $h^{-1/2}$ dependence. Thus

$$E^{lky}(h_2) = E^{lky}(h_1)[h_1/h_2]^{1/2}. \tag{10}$$

The refractive trapping of edge wave energy between depths h_1 and h_2 will reduce the amount of E^{fre} reaching h_2 by the factor L_{h_1,h_2}:

$$E^{fre}(h_2) = E^{fre}(h_1)[h_1/h_2]^{1/2} L_{h_1,h_2}. \tag{11}$$

Manipulation of equations (8*a*), (9), and (11) yields

$$L_{h_1,h_2} = \left[\frac{1-B(h_2)}{1-B(h_1)}\right]\left[\frac{E^{obs}(h_2)}{E^{obs}(h_1)}\right]\left[\frac{h_2}{h_1}\right]^{1/2}. \tag{12}$$

When B is small, as in the present case (Table 4), L_{h_1,h_2} is insensitive to large relative changes in B and is essentially a measure of the deviation of E^{obs} from an $h^{-1/2}$ leaky wave dependence.

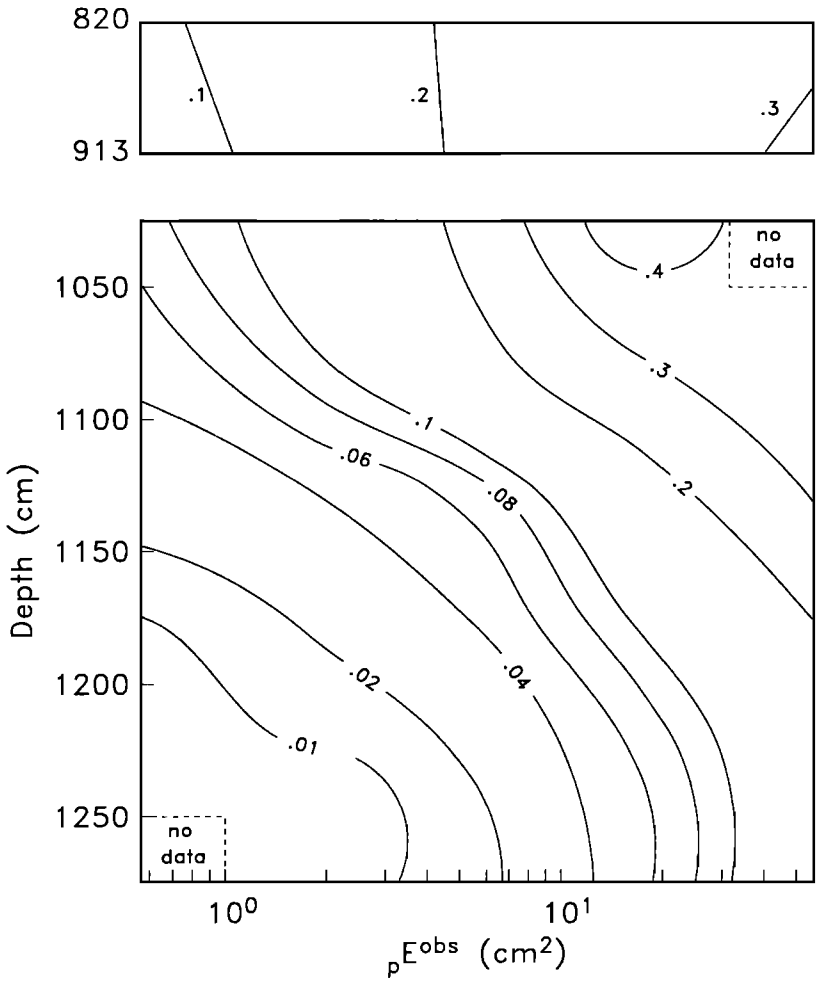

Fig. 8. Contours of $_pE^{bnd}/_pE^{obs}$, the ratio of predicted bound wave energy to observed infragravity energy as a function of depth and $_pE^{obs}$, at (top) Barbers Point and (bottom) Imperial Beach. Data were binned according to mean water depth (eight bins) and observed infragravity energy (five logarithmically spaced bins) and ratios averaged within a bin. The average ratios and number of observations in each bin are given in Table 3.

Substitution of observed values (Table 4) in equation (12) yields $L_{8.5,11.5} = 1.02$, $L_{8.5,183} = L_{11.5,183} = 0.07$. Virtually no free wave energy is trapped between 8.5- and 11.5-m depth, compared with greater than 90% between either shallow sensor and 183-m depth. Thus in 8- to 13-m depth, for E_{SS} ~1900 cm^2, an average of about 25% of the total infragravity energy is estimated to be bound (Table 4); ~5% is leaky (or of high mode number) and reaches 183 m depth, and 70% is trapped shoreward of 183 m. Frequency-wavenumber spectra from an array of pressure sensors in 8-m depth at Duck, North Carolina, also suggest the importance of edge waves well outside the surf zone [*Oltman-Shay et al.*, 1989; J. Oltman-Shay, personal communication, 1990].

The spatial variations of E^{bnd}, E^{lky}, and E^{edg} for idealized wave conditions are illustrated in Figure 11. E^{bnd} is calculated using equation (3) and the frequency spectrum shown in Figure 2 with $E_{SS} = 1800$ cm^2 (close to E_{SS} in Table 4) and full angular width of 40° (selected so the predicted and observed E^{bnd} in 11.5-m depth were approximately 6 cm^2; BE^{obs} in Table 4). E^{lky} for a typical infragravity frequency (0.02 Hz) and normal incidence is also shown in Figure 11. Shoreward of the turning

TABLE 3. Average Ratios $_pE^{bnd}/_pE^{obs}$ and Number of Observations in Each Bin in Figure 8

Depth, cm	$_pE^{obs}$, cm^2									
	0.0–1.0		1.0–3.16		3.16–10.0		10.0–31.6		31.6–100.0	
	Ratio	No.	Ratio	No.	Ratio	No.	Ratio	No.	Ratio	No.
820–849	0.09	71	0.15	73	0.22	20	0.25	14	0.26	3
850–913	0.08	117	0.13	187	0.21	42	0.22	25	0.36	5
1000–1049	0.07	9	0.13	13	0.23	6	0.46	2	...*	...
1050–1099	0.05	87	0.10	146	0.18	69	0.31	38	0.35	4
1100–1149	0.03	112	0.04	307	0.08	213	0.17	91	0.31	22
1150–1199	0.01	40	0.02	352	0.04	305	0.11	84	0.20	20
1200–1249	0.01	6	0.01	128	0.02	162	0.07	48	0.16	7
1250–1300	...	...	0.01	15	0.02	9	0.06	5	0.16	1

*No data.

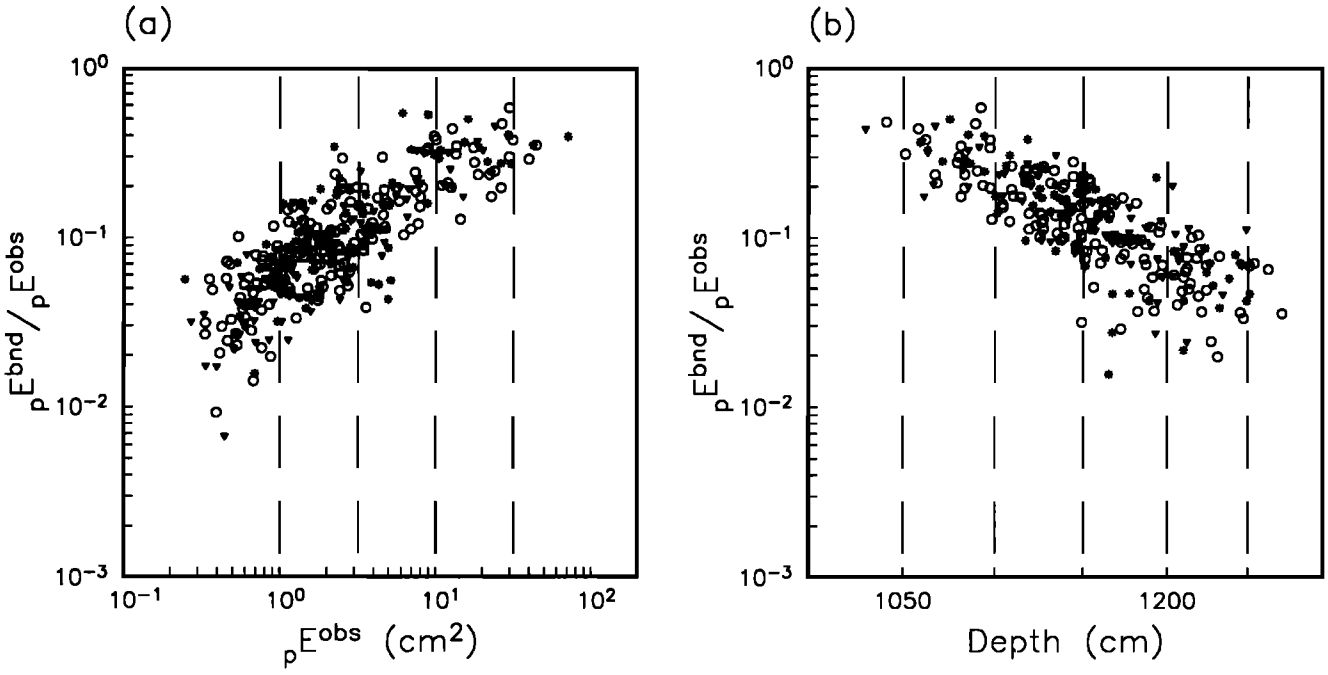

Fig. 9. The ratio of predicted bound wave to observed infragravity energy ($_pE^{bnd}/_pE^{obs}$), (*a*) as a function of $_pE^{obs}$ for the limited depth range 1050 – 1100 cm and (*b*) as a function of depth for a fixed range of $_pE^{obs}$ (10 – 32 cm^2). As in Figure 5, peak frequencies (f_p) of each record are $f_p \leq 0.067$ Hz (asterisks), $0.067 < f_p \leq 0.10$ Hz (circles) and $f_p > 0.10$ Hz (triangles). The dashed vertical lines indicate bin boundaries for the average ratios shown in Figure 8.

point (the most seaward edge wave antinode where exponential decay begins), $E^{edg} \sim E^{lky} \sim h^{-1/2}$, and beyond the turning point, $E^{edg} \sim e^{-2k_y x}$, where k_y is the longshore wavenumber and x is the cross-shore distance measured from the shoreline. Thus leaky and edge waves have similar spatial dependence shoreward of the edge wave turning point. The exponentially decaying edge wave tails in Figure 11 show that of the edge waves modes high enough ($n \geq 3$) to reach 8.5-m depth, only the amplitude of a mode 3 edge wave varies significantly over the depth range 8.5–11.5 m (for a frequency 0.02 Hz on a 0.02 slope). Mode numbers ≤7 are trapped shoreward of 183 m. The location and depth of a turning point depends on the edge wave mode number, frequency, and the beach slope but it is generally the case that many more modes have turning points between 11.5 and 183 m than between 8.5 and 11.5 m depths. E^{fre} in 11.5-m depth (Figure 11) is set equal to the observed value (E^{obs} (1-B) = 22 cm^2 from Table 4). The curves for E^{bnd} and E^{fre} are thus both constructed to match the observations in 11.5-m depth. The calculated $L_{8.5,11.5} \cong 1.0$ (equation (12) and Table 4) suggests little trapping of infragravity energy between depths of 8.5 and 11.5 m. On the other hand, E^{obs} at Point Conception is much larger than would occur with bound waves only, but much smaller than if all the free wave energy in shallow water radiated offshore. The calculated $L_{8.5,183} = L_{11.5,183} = 0.07$ essentially corresponds to the reduction of the Point Conception observation below the free wave curve in Figure 11. Although leaky (and very high-mode ($n > 7$) edge) wave energy is only a small fraction of E^{obs} in shallow water, it is sufficient to completely dominate the infragravity wave energy in 183-m depth.

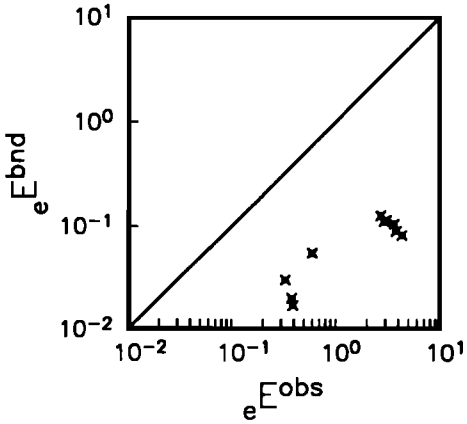

Fig. 10. Unidirectional bound wave model predicted infragravity sea surface elevation energy ($_eE^{bnd}$) versus observed infragravity sea surface elevation energy ($_eE^{obs}$) in 183-m depth at Point Conception. The solid line is $_eE^{bnd} = {}_eE^{obs}$.

Sand's [1982*b*] sea surface elevation observations in 40-m depth, yielding $E^{bnd}/E^{obs} \sim 1.0$, are much different from the

TABLE 4. Average Observed Infragravity Energy $\langle E^{obs} \rangle$ and Average Bound Fraction $B = \langle E^{bnd}/E^{obs} \rangle$ for Similar Average Sea Swell Energy $\langle E_{SS} \rangle$

Site	Mean Depth m	No. of Records	$\langle E_{SS} \rangle$ cm^2	$\langle E^{obs} \rangle$ cm^2	$\langle E^{bnd}/E^{obs} \rangle$
B.P.	8.5	91	1950	35	0.28
I.B.	11.5	13	1830	28	0.21
P.C.	183	4	1840	0.43	0.07

Data from each site are averaged together. Sites are identified in the footnote to Table 2.

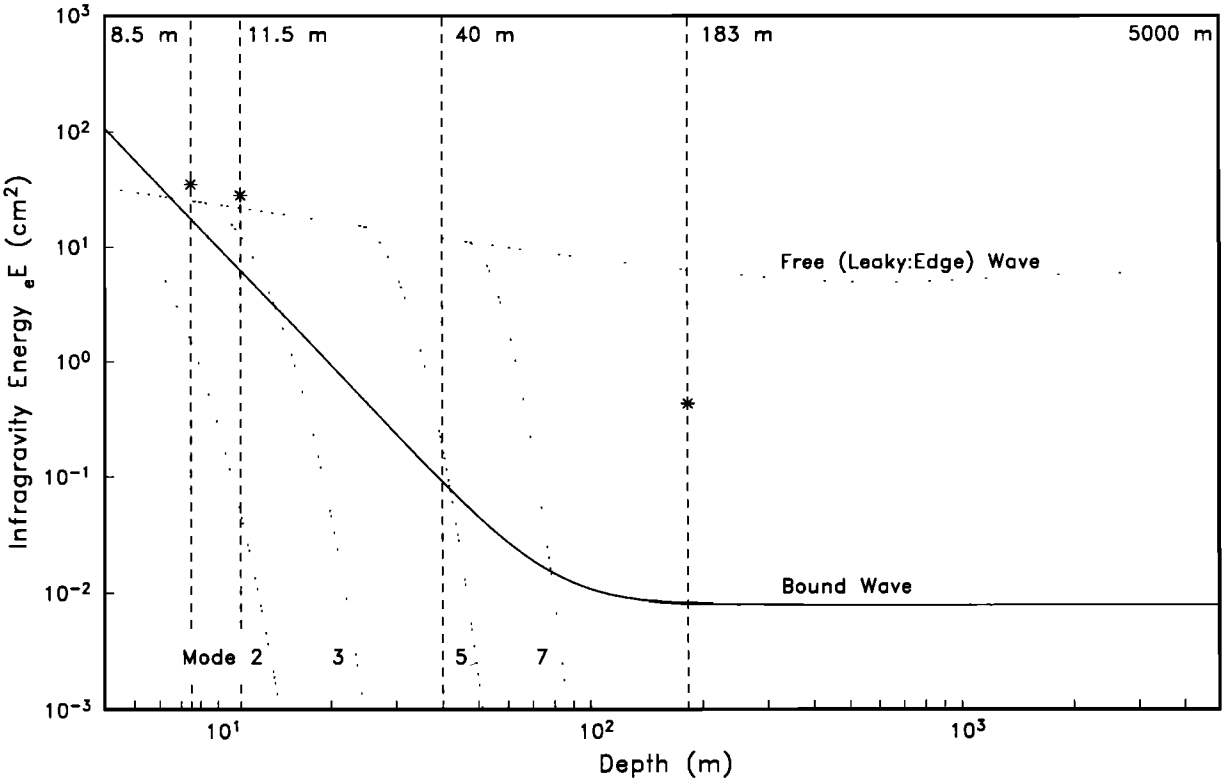

Fig. 11. Infragravity wave forms. The solid line is the bound wave energy forced by a sea and swell spectrum (E_{SS} = 1800 cm^2 and f_p = 0.067 Hz) with a constant 40° angular width. Leaky wave and edge wave energy envelopes at 0.02 Hz on a bottom slope of 0.02 are shown by dotted lines. The leaky:edge wave curve is constructed such that the ratio of bound wave energy to the total (leaky:edge + bound) infragravity energy is ~0.2 in 11.5 m. The leaky:edge wave energy at other depths is obtained from linear conservation of energy. Leaky and edge wave curves are similar shoreward of the exponentially decaying edge wave tails, shown for modes 2, 3,5, and 7. The asterisks indicate the average observed infragravity energy (E^{obs}) at each site, for sea and swell spectra with E_{SS} ~1900 cm^2 (Table 4). The depths discussed in the text are shown by vertical dashed lines.

present ratios showing a maximum value of 0.15 in 12.5-m depth and a decrease with increasing depth (Figure 8). This discrepancy may be due to a number of factors. First, Sand's predicted E^{bnd} was calculated assuming unidirectional sea and swell waves, which overestimates E^{bnd} and E^{bnd}/E^{obs}. Although the very strong effects of directional spreading are reduced in deep water compared with shallow water, an angular spread of 40° reduces the predicted E^{bnd} by about a factor of 6 (Table 1). This is significant and may explain the large differences (at least a factor of 5) with the present observations. However, differences in the sites and E_{SS} are probably also important. Sand's observations were from the middle of the North Sea, about 200 km from the nearest coastline, presumably reached only by leaky waves. Thus edge waves present at the current sites (on the continental shelf and in Hawaii) may not have occurred in Sand's observations, and bound waves were thus relatively more important. Additionally, E^{bnd}/E^{obs} increases with increasing E_{SS} (at least in shallow water; Figure 8) and E_{SS} ~26,000 cm^2 (H_{SS} ~650 cm!) in the North Sea data, considerably larger than the maximum E_{SS} ~5000 cm^2 in the present data sets (Figure 5). Negligible E^{edg} and large E_{SS} may have increased the relative importance of bound waves in the North Sea.

At 5000-m depth in the North Atlantic ~500 km from the nearest coastline, *Webb et al.* [1991] found that E^{obs} on the seafloor was correlated not with the local E_{SS} but with E_{SS} averaged over all coastlines within the "line of sight" of the experiment site. The correlations occur because locally forced bound waves are too short to penetrate the water column and $_pE^{obs}$ is due predominantly to free infragravity energy E^{fre}, radiated from sometimes distant coastal areas with energetic sea and swell [*Webb et al.*, 1991]. In contrast, infragravity waves measured on the seafloor in 4000-m depths 200 km offshore of Point Arena, California [*Sutton et al.*, 1965], and at the sea surface in 183-m depth 10 km west of Point Conception were correlated with the local E_{SS} even though bound waves are not important in either data set. E^{obs} and local E_{SS} are probably correlated because the local E_{SS} is highly correlated with E_{SS} at nearby coastal sites radiating free infragravity energy, and the decrease in E^{fre} due to radial spreading is minimal because of the proximity of these sites to the coast. In 5000-m depth, 1000 km from the coast and due west of the 183-m depth site of the present study, directional spectra [*Webb et al.*, 1991] do in fact show significant infragravity energy propagating from the California coast near Point Conception, where surface wave energy is consistently high. The present Point Conception data set contains no cases of small E_{SS}, so radiation from the nearby coast is presumably always significant and more important than radiation from distant coasts. In both the North Atlantic (with E_{SS} a line of sight average, Webb *et al.*, 1991) and offshore of Point Conception in the Pacific, a very small fraction of E_{SS} is radiated from coastal regions as leaky (and/or very high mode edge) infragravity energy.

Third Moments

Theoretically, infragravity bound waves generated by nonlinear difference interactions are phase coupled to pairs of free waves (sea and swell) and 180° out of phase with the wave group envelope (for narrow free wave directional distributions; negative C in Figure 1). This coupling produces negative skewness.

TABLE 5. Average Skewness Values for 34-min-Long Records

Site	Depth, m	No. of Records	Skewness	
			$1.5 f_p$	Nyquist
B.P.	8.2 – 9.1	557 (76)	-0.08 (-0.15)	0.12 (0.28)
I.B.	10.2 – 11.0	479 (103)	-0.09 (-0.15)	0.02 (0.04)
I.B.	11.1 – 11.8	1313 (233)	-0.07 (-0.14)	0.02 (0.03)
I.B.	11.9 – 12.7	509 (82)	-0.06 (-0.14)	0.01 (0.03)
P.C.	183	10 (10)	0.003 (0.003)	0.08 (0.08)

The upper limits of frequencies included in the calculations are indicated in the heading of the skewness columns. The Nyquist frequency was 1.0 Hz at Point Conception (P.C.) and 0.5 Hz at Barbers Point (B.P.) and Imperial Beach (I.B.). Energy at frequencies greater than the upper limit was set to zero. Values in parentheses are for the larger waves ($E_{SS} \geq 625$ cm).

Coupling between sea and swell and higher-frequency waves forced by sum interactions produces positive skewness [*Hasselmann et al.*, 1963].

Data from all three field sites were divided into 34-min segments. To reduce the effects of high-frequency bound harmonics on skewness, each record was low-pass filtered by setting equal to zero the Fourier coefficients of sea surface elevation at frequencies greater than 1.5 times the power spectral peak. After an inverse Fourier transform, the skewness was calculated in the time domain. Skewness was also calculated without low-pass filtering, thus including both high- and low-frequency bound waves. As shown in Table 5, the skewness of the low-passed data is negative at the shallow depths (8–13 m), consistent with the theoretically expected coupling between sea and swell and infragravity bound waves, and close to zero in deep water (183-m depth) as expected for uncoupled infragravity waves. The magnitude of the skewness in shallow water increases when the low-energy records ($E_{SS} <$ 625 cm^2) are excluded (Table 5). Although the near-zero band-passed skewness in 183-m depth is consistent with negligible E^{bnd}, it must be interpreted cautiously. In this depth, $\omega_n (h/g)^{1/2} \sim 2$, directional spreads may be large, and bound infragravity waves may contribute either positive or negative skewness (Figure 1). Zero skewness could thus also result from canceling contributions.

In shallow water the band-passed skewness ($1.5 f_p$ column in Table 5) is negative while the total (Nyquist) skewness is positive. The positive skewness due to bound high-frequency harmonics is significantly offset by negative skewness from bound infragravity waves, similar to results from the surf zone [*Elgar and Guza*, 1985]. The cancellation is nearly complete at Imperial Beach, where positive and negative contributions of about |0.1| yield a total skewness of roughly 0.03.

Bispectral analysis [*Hasselmann et al.*, 1963] indicates the contribution to third moments from individual triads of infragravity and sea and swell frequencies. The normalized magnitude of the bispectrum, the bicoherence (b), indicates the relative degree of phase coupling between frequencies. The biphase gives the phase relationship between the coupled waves. The same 34-min records for which skewness was calculated were analyzed using bispectral techniques. An example from Imperial Beach (Figure 12) shows that infragravity energy is significantly coupled to higher-frequency sea and swell within the power spectral peak ($0.05 \leq f \leq 0.09$ Hz). The biphases (not shown) are between 158° and 176°. Figure 12 is typical of cases with energetic swell and infragravity waves in relatively shallow water (4- to 13-m depth).

In relatively deep water (183 m; offshore of Point Conception) bispectra do not show statistically significant coupling between sea and swell and infragravity waves, consistent with our result that bound waves make a very small contribution to the observed infragravity wave spectrum.

6. SUMMARY

The sensitivity of the predicted [*Hasselmann*, 1962] infragravity bound wave energy (E^{bnd}) to variations in depth and sea and swell conditions was examined and E^{bnd} was compared with the observed infragravity energy (E^{obs}) in both 8- to 13-m and 183-m water depths.

E^{bnd} varies considerably with changes in the depth, the free wave (sea and swell) frequencies, and free wave angular spread. With the same sea and swell spectrum, E^{bnd} in shallow (O(10 m)) and deep (O(200 m)) water can differ by 10^4 (Figures 2 and

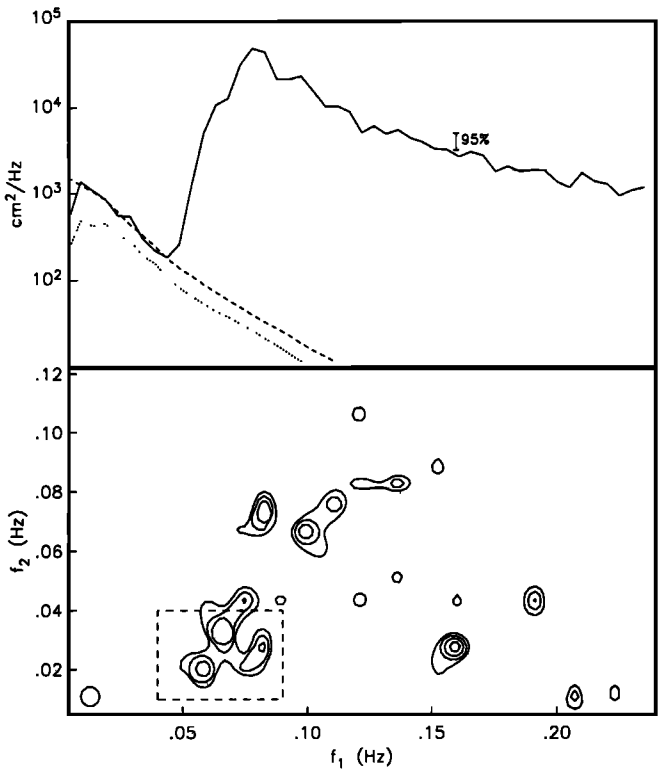

Fig. 12. (top) Energy spectra and (bottom) contours of bicoherence (24 DOF) in 10.9-m depth at Imperial Beach (January 14, 1990, 1948). Observed sea and swell surface elevation spectrum (solid line, $f \geq 0.04$ Hz), observed infragravity pressure spectrum (solid line, $f <$0.04 Hz), unidirectional bound wave model pressure spectrum (dashed line), and $\cos^{2s}$ model pressure spectrum (dotted line) are shown ($E_{SS} =$ 1618 cm^2, $E^{obs} =$ 27 cm^2, $E^{bnd} =$ 31 and 13 cm^2 for unidirectional and directional model, respectively). The minimum bicoherence-contour level plotted is significant at the 95% level [*Haubrich*, 1965], $b =$ 0.50, with additional contours every 0.1. The convention is that the interacting frequencies are f_1, f_2, $f_1 + f_2$, with $f_1 \geq f_2$; thus the lowest frequency is f_2 and the bicoherence enclosed in the dashed box indicate coupling between infragravity waves ($f_2 <$0.04 Hz) and waves with frequencies within the power spectral peak (0.04 Hz $< f_1, f_1 + f_2 <$0.12 Hz).

3). E^{bnd} in shallow (relative to a sea and swell wavelength) water is particularly sensitive to changes in the angular spread between interacting free waves (Figure 2*a*). In O (10 m) depth, even slight directional spreading of the sea and swell spectrum reduces E^{bnd} to 10% of the value predicted with a unidirectional wave field. In contrast, the bound wave coupling coefficient in deep water has the largest magnitude for large angular spread (Figure 1*b*) and a directionally broad sea and swell spectrum can force more bound wave energy than a relatively narrow one (Figures 2*c* and 2*d*). Directionally spread seas in deep water may excite "short" (high wavenumber) infragravity waves. Because these short infragravity waves will not penetrate deeply into the water column, infragravity energy measured at the sea surface in deep water can be radically different from infragravity energy measured on the seafloor or even a few hundred meters below the surface. Bound wave energy is also a strong function of the free wave frequencies. In shallow water, E^{bnd} forced by low-frequency (O (0.07 Hz)) swell is 10^2 times larger than E^{bnd} forced by equally energetic high-frequency (O (0.2 Hz)) seas (Figure 3). In deep water, high-frequency seas force more E^{bnd} at the sea surface than swell, although the differences (sea versus swell) in E^{bnd} energy are smaller than in shallow water.

E^{obs} from three sites in 8- to 183-m depth were compared with E^{bnd} predictions based on unidirectional and directional bound wave theory. Low-resolution frequency-directional incident wave spectra were estimated using a small 6 m x 6 m slope array. In ~8-m depth at Barbers Point, the unidirectional E^{bnd} is frequently greater than E^{obs} and exceeds the directional E^{bnd} by as much as a factor of 20 (Figures 5, 7*b*, and 7*d*). Directional spreading of the incident wave field must be included when applying bound wave theory in shallow water. The ratio E^{bnd}/E^{obs}, the fraction of the infragravity energy which is bound, varies with depth and sea and swell energy (E_{SS}). The portion of E^{obs} accounted for using directional bound wave theory ranges from less than 0.01 in 13-m depth with small E_{SS} to ~0.4 in 8-m depth with large E_{SS} (Figure 8). In 183-m depth ~10 km offshore of Point Conception, unidirectional E^{bnd} is less than 10% of E^{obs}, even with large E_{SS} (Figures 5 and 10). The estimates of E^{bnd} are qualitative because of uncertainties in the sea and swell directional spread, but also because in shallow depths the theoretical assumptions of small Ursell number and a slowly varying wave field may be violated. However, small E^{bnd}/E^{obs} ratios occur in all depths and show systematic variations which cannot be attributed to the low resolution of the sea and swell directional spectrum. Free infragravity waves, either leaky waves or edge waves, are more energetic than bound waves at both the shallow and deep sites. The low level of infragravity energy observed in 183-m depth compared with 8- to 13-m depths, with similarly moderate sea and swell energy, suggests that leaky (and very high mode edge) waves contribute less than 10% of the infragravity energy in 8–13 m. Most of the free infragravity wave energy in shallow water is refractively trapped and does not reach the deep site (Figure 11). At all of the sites and depths considered, E^{bnd} and E^{obs} were highly correlated, suggesting a strongly related generation mechanism for free and bound infragravity waves. Bound waves in shallow water may indeed be a source of free infragravity waves, as suggested by Longuet-Higgins & Stewart [1962].

APPENDIX

The first two Fourier coefficients $a_1(f)$, $b_1(f)$ of the frequency-directional spectrum were estimated from the slope array cross spectra [*Herbers and Guza*, 1989]. Following *Kuik et al.* [1988], at each frequency the mean direction $\theta_0(f)$ is

$$\theta_0(f) = \arctan\left[\frac{b_1(f)}{a_1(f)}\right] \tag{A1}$$

and the rms angular deviation of energy from the mean direction is (for narrow distributions),

$$\sigma(f) = \left[\int_{\theta_0-\pi}^{\theta_0+\pi} (\theta-\theta_0)^2 D(f,\theta)\,d\theta\right]^{1/2} = [2(1-m_1)]^{1/2} \tag{A2}$$

where

$$m_1 = [a_1(f)^2 + b_1(f)^2]^{1/2}. \tag{A3}$$

The directional distribution was modeled as the widely used parametric form

$$D(f,\theta) = C(f)\cos^{2s(f)}\left[\frac{\theta-\theta_0(f)}{2}\right], \tag{A4}$$

where $C(f)$ is a normalization constant and the spreading parameter $s(f)$ was selected [*Kuik et al.*, 1988, equation 38] so that $D(f,\theta)$ (equation (A4)) had directional width equal to $\sigma(f)$ (equation (A2)):

$$s(f) = \left[\frac{2}{\sigma(f)^2} - 1\right]. \tag{A5}$$

Acknowledgments. This work has been supported by the U.S. Army Corps of Engineers Civil Research Unit 22119 as part of the Monitoring Completed Coastal Projects Program through the U.S. Army Engineer Waterways Experiment Station, Coastal Engineering Research Center, and by the Coastal Sciences Branch of the Office of Naval Research. Permission was granted by the Chief of Engineers to publish this paper. The staff of the Coastal Data Information Program (supported by the U.S. Army Corps of Engineers and the California Department of Boating and Waterways) installed and maintained the arrays at Barbers Point and Imperial Beach. Marisco, Inc., and Sea Engineering, Inc., assisted in the deployment of instruments at Barbers Point. Thanks to Chevron Oil Field Research Company for providing the data from the platform *Hermosa*. Thanks to T. H. C. Herbers for many helpful discussions and assistance, and S. Elgar for helpful suggestions and use of his bispectral computer code. S. Elgar, T. H. C. Herbers and J. Oltman-Shay generously shared the results of their analysis of infragravity waves at Duck, North Carolina (in advance of publication of those results), thus contributing significantly to the present study.

REFERENCES

Biesel, F., Equations générales au second ordre de la houle irrégulière, *Houille Blanche*, *7*, 372–376, 1952.

Bowen, A. J., and R. T. Guza, Edge waves and surf beat, *J. Geophys. Res.*, *83*(C4), 1913–1920, 1978.

Elgar, S., and R. T. Guza, Observations of bispectra of shoaling surface gravity waves, *J. Fluid Mech.*, *161*, 425–448, 1985.

Elgar, S., J. Oltman-Shay, and P. Howd, Observations of infragravity-frequency long waves, I, Coupling to wind waves (abstract), Eos Trans. *AGU*, *70*(43), 1133, 1989.

Elgar, S., T. H. C. Herbers, M. Okihiro, J. Oltman-Shay, and R. T. Guza, Observations of infragravity waves, *J. Geophys. Res.*, in press, 1992.

Funke, E. R., and E. P. D. Mansard, On the synthesis of realistic sea states in a laboratory flume, Rep. LTR HY 66, Natl. Res. Counc., Ottawa, Canada, 1979.

Gallagher, B., Generation of surf beat by non-linear wave interactions, *J. Fluid Mech.*, *49*, 1–20, 1971.

Goda, Y., Irregular wave deformation in the surf zone, *Coastal Eng. Jpn.*, *18*, 13–26, 1975.

Goodman, D., T. Yamamoto, M. Trevorrow, C. Abbot, A. Turgut, M. Badley, and K. Ando, Directional spectra observations of seafloor microseisms from an ocean-bottom seismometer array, *J. Acoust. Soc. Am.*, *86*(6), 2309–2317, 1989.

Guza, R. T., E. B. Thornton, and R. A. Holman, Swash on steep and shallow beaches, *Proc. Int. Coastal Eng. Conf.*, *19th*, 708–723, 1984.

Guza, R. T., and E. B. Thornton, Observations of surf beat, *J. Geophys. Res.*, *90*(C2), 3161–3172, 1985.

Hasselmann, K., On the non-linear energy transfer in a gravity-wave spectrum, 1, General theory, *J. Fluid Mech.*, *12*, 481–500, 1962.

Hasselmann, K., W. Munk, and G. MacDonald, Bispectra of ocean waves, in *Time Series Analysis*, edited by M. Rosenblatt, Ed., pp. 125–139, John Wiley, New York, 1963.

Haubrich, R. A., Earth noises, 5 to 500 millicycles per second, *J. Geophys. Res.*, *70*(6), 1415–1427, 1965.

Herbers, T. H. C., and R. T. Guza, Estimation of wave radiation stresses from slope array data, *J. Geophys. Res.*, *94*(C2), 2099–2104, 1989.

Holman, R. A., Infragravity energy in the surf zone, *J. Geophys. Res.*, *86*(C7), 6442–6450, 1981.

Holman, R. A., and A. H. Sallenger, Jr., Setup and swash on a natural beach, *J. Geophys. Res.*, *90*(C1), 945–953, 1985.

Howd, P., J. Oltman-Shay, and R.A. Holman, Wave variance partioning in the trough of a barred beach, *J. Geophys. Res.*, *96*(C7), 12,781–12,795, 1991.

Huntley, D. A., Long period waves on a natural beach, *J. Geophys. Res.*, *81*(36), 6441–6449, 1976.

Huntley, D. A., and C. S. Kim, Is surf beat forced or free?, *Proc. Int. Coastal Eng. Conf., 19th*, 871–885, 1984.

Huntley, D. A., R. T. Guza, and E. B. Thornton, Field observations of surf beat, 1. Progressive edge waves, *J. Geophys. Res.*, *86*(C7), 6451–6466, 1981.

Kostense, J. K., Measurements of surf beat and set-down beneath wave groups, *Proc. Int. Coastal Eng. Conf., 19th*, 724–740, 1984.

Kuik, A. J., G. P. Van Vledder, and L. H. Holthuijsen, A method for the routine analysis of pitch-and-roll buoy wave data, *J. Phys. Oceanogr.*, *18*, 1020–1034, 1988.

List, J. H., Wave groupiness as a source of nearshore long waves, *Proc. Int. Coastal Eng. Conf., 20th*, 497–511, 1986.

Longuet-Higgins, M. S., A theory of the origin of microseisms, *Philos. Trans. R. Soc. London, Ser. A*, *243*, 1–35, 1950.

Longuet-Higgins, M. S., and R. W. Stewart, Changes in the form of short gravity waves on long waves and tidal currents, *J. Fluid Mech.*, *8*, 565–583, 1960.

Longuet-Higgins, M. S., and R. W. Stewart, Radiation stress and mass transport in gravity waves, with application to 'surf-beats,' *J. Fluid Mech.*, *13*, 481–504, 1962.

Longuet-Higgins, M. S., and R. W. Stewart, Radiation stresses in water waves: A physical discussion, with applications, *Deep Sea Res.*, *11*, 529–562, 1964.

Mansard, E. P. D., and V. Barthel, Shoaling properties of bounded long waves, *Proc. Int. Coastal Eng. Conf., 19th*, 798–814, 1984.

Meadows, G. A., R. A. Shuchman, and J. D. Lyden, Analysis of remotely sensed long-period wave motions, *J. Geophys. Res.*, *87*(C8), 5731–5740, 1982.

Medina, J. R., Discussion, The dependency of inshore long waves on the characteristics of offshore short waves, by R. C. Nelson, P. D. Treloar and N. V. Lawson, *Coastal Eng.*, *14*, 185–190, 1990.

Middleton, J. H., M. L. Cahill, and W. W. Hsieh, Edge waves on the Sydney coast, *J. Geophys. Res.*, *92*(C9), 9487–9493, 1987.

Munk, W. H., Surf beats, Eos Trans. *AGU*, *30*(6), 849–854, 1949.

Nelson, R. C., P. D. Treloar, and N. V. Lawson, The dependency of inshore long waves on the characteristics of offshore short waves, *Coastal Eng.*, *12*(3), 213–231, 1988.

Oltman-Shay, J., and R. T. Guza, Infragravity edge wave observations on two California beaches, *J. Phys. Oceanogr.*, *17*(5), 644–663, 1987.

Oltman-Shay, J., S. Elgar, and P. Howd, Observations of infragravity-frequency long waves, II. Comparisons with a 2-D wave group generation model (abstract), Eos Trans. *AGU*, *70*(43), 1133, 1989.

Ottesen Hansen, N.-E., Long period waves in natural wave trains, *Prog. Rep. 46*, Inst. Hydrodyn. and Hydraulic Eng., Techn. Univ. Denmark, 13–24, 1978.

Sand, S. E., Long waves in directional seas, *Coastal Eng.*, *6*(3), 195–208, 1982*a*.

Sand, S. E., Wave grouping described by bounded long waves, *Ocean Eng.*, *9*(6), 567–580, 1982*b*.

Sasaki, T., and K. Horikawa, Observation of nearshore current and edge waves, *Proc. Int. Coastal Eng. Conf., 16th*, 791–809, 1978.

Sasaki, T., K. Horikawa, and S. Hotta, Nearshore current on a gently sloping beach, *Proc. Int. Coastal Eng. Conf., 15th*, 626–644, 1976.

Suhayda, J. N., Standing waves on beaches, *J. Geophys. Res.*, *79*(21), 3065–3071, 1974.

Sutton, G. H., W. G. McDonald, D. D. Prentiss, and S. N. Thanos, Ocean-bottom seismic observatories, *Proc. IEEE*, *53*(12), 1909–1921, 1965.

Symonds, G., D. A. Huntley, and A. J. Bowen, Two-dimensional surf beat: Long wave generation by a time-varying breakpoint, *J. Geophys. Res.*, *87*(C1), 492–498, 1982.

Tucker, M. J., Surf beats: Sea waves of 1 to 5 minute period, *Proc. R. Soc. London, Ser. A*, *202*, 565–573, 1950.

Webb, S.C., X. Zhang, and W. Crawford, Infragravity waves in the deep ocean, *J. Geophys. Res.*, *96*(C2), 2723–2736, 1991.

R. T. Guza, M. Okihiro, and R. J. Seymour, Scripps Institution of Oceanography, 0222, University of California, San Diego, La Jolla, CA 92093-0222.

(Received May 22, 1991;
revised February 4, 1992;
accepted February 4, 1992.)